Metals and Materials International (2020) 26:1099–1133
https://doi.org/10.1007/s12540-019-00565-z

Manufacturing Methods, Microstructural and Mechanical Properties Evolutions of High-Entropy Alloys: A Review

Yaser A. Alshataif[1] · S. Sivasankaran[1] · Fahad A. Al-Mufadi[1] · Abdulaziz S. Alaboodi[1] · Hany R. Ammar[1,2]

Received: 26 August 2019 / Accepted: 29 November 2019 / Published online: 6 December 2019

Abstract

High entropy alloys (HEAs) are being attracted recently by several researchers, scientists, and academicians to achieve extraordinary and outstanding properties that cannot be obtained from conventional alloys. HEAs are multicomponent alloys in which a minimum of five metallic elements are mixed in an equal molar or non-equal molar ratio. The rapid growth of this field produces a huge amount of scientific papers over the last decade. However, still, there is a need to review various manufacturing methods and their results. Also, the outcome of the scientific articles related to HEAs has ignored the various methods of synthesizing and manufacturing. In this review article, an attempt was made and largely concentrated on the methods and techniques that can be used in the manufacturing and synthesizing of the HEAs. Recently, the properties of HEAs become much better when compared to conventional alloys. Some techniques have succeeded in producing ultrafine microstructure grains which become a leap in industrial fields. Now, the manufacturing methods of conventional alloys are almost familiar and implemented according to the suggestions given by the researchers and academicians based on their work. Therefore, the present review article has demonstrated various methods of manufacturing of HEAs with novel schematics with a preview description for more understanding of the basic work criteria. Besides, this article has reviewed the outcomes of several research articles related to several methods, then compared the outcome of each method with the corresponding mechanical properties, and major challenges of HEAs are discussed and reported.

Keywords High-entropy alloys · Synthesis methods · Microstructure · Mechanical properties · Challenges

Electronic supplementary material The online version of this article (https://doi.org/10.1007/s12540-019-00565-z) contains supplementary material, which is available to authorized users.

✉ S. Sivasankaran
sivasankarangs1979@gmail.com; sivasankaran@qec.edu.sa; s.udayar@qu.edu.sa

Yaser A. Alshataif
yasserahmedalshoteef@gmail.com

Fahad A. Al-Mufadi
almufadi@qec.edu.sa

Abdulaziz S. Alaboodi
alaboodi@qec.edu.sa

Hany R. Ammar
hanyammar@qec.edu.sa

[1] Mechanical Engineering Department, Qassim University, Buraidah 51452, Saudi Arabia

[2] Metallurgical and Materials Engineering Department, Faculty of Petroleum and Mining Engineering, Suez University, Suez 43721, Egypt

Abbreviations

SPD	Sever plastic deformation process
CGs	Coarse grains
HEBM	High energy ball milling
HEAs	High entropy alloys
MCAs	Multi component alloys
CAs	Conventional alloys
SS	Solid solution
IMEs	Intermetallic elements
YS	Yield strength
VAM	Vacuum arc melting
SMs	Strengthening mechanisms
SSP	Solid state processing
LSP	Liquid state processing
TFD	Thin film deposition
AMT	Additive manufacturing technology
SPS	Solid state processing
PCA	Process control agent
HP	Hot pressing
FCC	Face centered cubic
BCC	Body centered cubic

HCP	Hexagonal closed pack
SEM	Scanning electron microscope
TEM	Transmission electron microscope
PECS	Pulsed electric current
DC	Direct current
UFG	Ultra-fine grain
CP	Cold pressing
VS	Vacuum sintering
AM	Arc melting
VHS	Vickers hardness strength
HP	Hot pressing
VHP	Vacuum hot pressing
UTS	Ultimate tensile strength
IMCs	Intermetallic compounds
HIP	Hot iso-static pressing
PM	Powder metallurgy
VIM	Vacuum induction melting
DS	Directional solidification
EMS	Electromagnetic stirring
MSD	Magnetron sputtering deposition
PLD	Pulsed laser deposition
PSD	Plasma spraying deposition
PVD	Physical vapor deposition
RHEA	Refractory high entropy alloy
HEATFs	High entropy alloy thin films
SLS	Selective laser sintering
SLM	Selective laser melting
SEBM	Selective electron beam melting
VED	Volumetric energy density
FWHM	Full width half maximum
XRD	X-ray diffraction
EBSD	Electron backscattered diffraction
DLF	Direct laser fabrication

1 Introduction

Nowadays, new materials with high demands are required in different applications such as transportation, energy, aerospace, medicine, and industrial approaches. In these fields, it is necessary to meet the desired mechanical properties such as the optimum strength, the hardness, the toughness, the ductility, the wear resistance, the thermal resistance, and the creep resistance [1]. Therefore, many methods and techniques have used to develop and improve the performance of materials either by breaking up the original grain and refined it like a severe plastic deformation process (SPD). In other words, the reduction of grains from coarse grains (CGs) of powder particles could be achieved by high-energy ball milling (HEBM) which can produce high entropy alloys (HEAs) by mixing of several elemental powders. Multicomponent alloys (MCAs) concept has begun back in the 1970s by undergraduate thesis and then, the work was carried out by another undergraduate student in 1998 tail by Huang [2]. Yeh et al. [3–5] have worked in MCAs and introduced the name as HEAs in the year 2004. The authors have defined that the HEAs are the alloys which consist of five or more principal elements in which the volume fraction of each element is in the range of 5%–35%. Also, HEAs have high mixing entropy in their liquid state or solid solution (SS) state at high temperatures [4, 5] when compared to the conventional alloys (CAs). In the CAs, one or two primary elements have presented and in some cases, a small number of additional elements have alloyed to improve their mechanical properties with improved microstructural features. The number of elements in the CAs usually produces some unwanted intermetallic phases which result to enhance the strength and decrease the ductility [6].

It is well known that a structural/tool material must possess superior properties even at a very high temperature which is the major demand for most of the modern industries. Basically, HEAs exhibits a magnificent properties such as excellent softening resistance at high temperatures [7, 8], retaining the high hardness at elevated temperature [9–12], superior wear resistance [13, 14] outstanding thermal stability [15], good oxidation [16, 17], elevated corrosion resistance [14, 18], and sluggish diffusion kinetics [19, 20]. Recently, several researchers have focused their research work on HEAs. Figure 1 shows the number of publications related to HEAs by year-wise which explains clearly the number of publications increases drastically [21]. Further, the concept of HEAs in the form of a senary system (mixing of six elements) as an example is illustrated in Fig. 2. Figure 2 shows the six elements in equiatomic ratio before mixing and after mixing to have a random SS which has high configurational entropy.

In the medical industry, Alagarsamy et al. [22] have used the HEA of $Al_{0.1}$CoCrFeNi for peripheral vascular stent application. The results explained that the $Al_{0.1}$CoCrFeNi HEA has possessed superior mechanical behavior compared to SS 316L steel; which is commonly used currently in the peripheral vascular stent. Synthesizing of HEAs from refractory elements such as Ti, Cr, Mn, Mo, W, Ta etc. to have excellent in ductility, more in strength, exceptional heat resistance, and wear resistance have investigated recently by the research community [23, 24]. An outstanding compressive yield strength (YS) was achieved from refractory based HEAs of HfMoTaTiZr and HfMoNbTaTiZr for 5.4 GPa and 5.05 GPa respectively which was investigated by Juan et al. [25]. These alloys were produced by vacuum arc melting (VAM) method. The main challenge in the refractory based HEAs is its high density which affects directly the strength-to-weight ratio. But this drawback can be overcome by adding light density material to the alloy. Several authors have attempted to develop various HEAs recently. However, there is no much

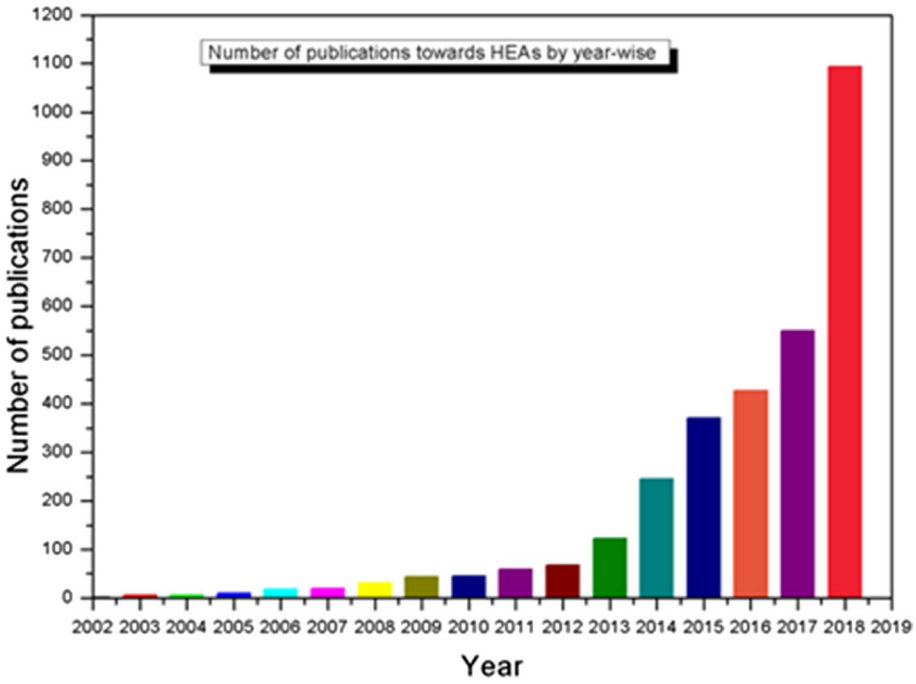

Fig. 1 Number of publications related to HEAs in year-wise across the world (Murty et al. [21])

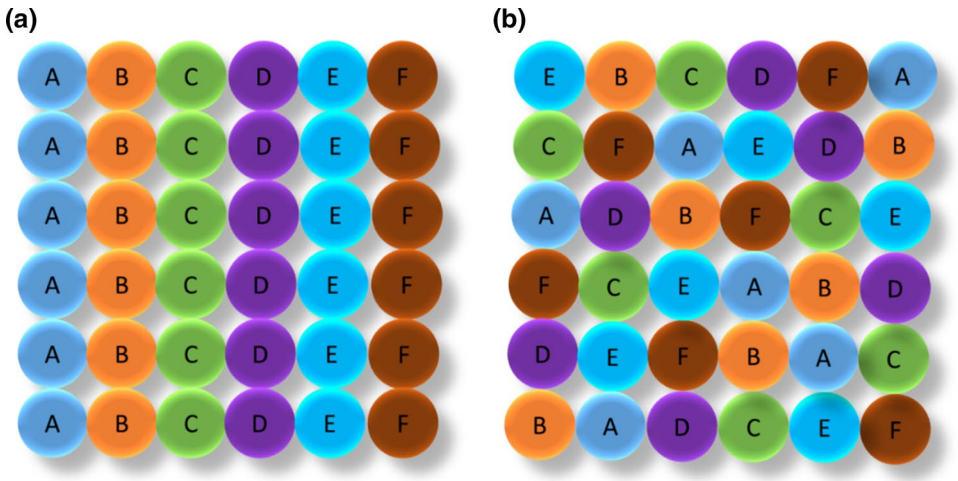

Fig. 2 Senary system-six elements in the equiatomic ratio: **a** before mixing; and **b** random solid solution after mixing to form HEA which has high configurational entropy

literature to examine the various manufacturing methods and issues related to HEAs. It is very difficult to categories the processes to be used for HEAs and its recommendations to the diversity field for fast-growing manufacturing sectors. Therefore, the main objectives of this review article are: (1) summarize the various processes to be used for HEAs starting from the alloy preparation with appropriate schematics and flow charts (2) microstructural changes, and mechanical properties improvement, (3) various outcomes from several HEAs investigated recently by several authors, (4) several challenges on processing of HEAs, and (5) issues and applications of HEAs. In this article, the HEAs fabrication technology were categorized into four, namely, solid-state processing (SSP) techniques [26–29], liquid state processing (LSP) [10, 30, 31], thin-film deposition (TFD) techniques, and additive manufacturing technology (AMT).

2 Solid-State Processing of HEAs

Most of the polycrystalline materials are synthesized through the SSP technique in which the mixing of several alloying elements is carried out at room temperature followed by consolidation at an elevated temperature. Figure 3 shows the schematic of the SSP route that can be used for the manufacturing of HEAs. In overall, the SSP

technique includes the powder production (Atomization and HEBM), mixing of powders (ball mill), consolidation of powders into the bulk sample (spark plasma sintering (SPS), hot pressing (HP), cold compaction), and various secondary operations (machining, extrusion and rolling).

2.1 Powder Atomization Method

Powder atomization is the one technique in which the molten metallic materials are directly converted into solid powder particles by gas or liquid stream. Figure 4 shows the schematic of the powder atomization process. Atomization device is usually consisting of two-stage: the first one is the furnace chamber in which the metallic powders called the charge are melt in a vacuum atmosphere to the required temperature, then the second one is the molten melt liquid drain through a nozzle which is located at the bottom of the tundish into atomizing chamber. As the molten melt continuously flows inside the tundish by gravity, the atomizing nozzle has disintegrated the liquid stream of melt into tiny droplets by high-pressure gas or water jet; which then solidified immediately (Fig. 4) led to form sold powder particles. The metal powders particle size is affected by the coolant distance, coolant pressure, coolant velocity, coolant mass flow rate, liquid stream velocity, and liquid mass flow rate, angle of impingement, superheat, metal surface tension and metal meting range [32]. Table 1 shows the range of those variables to be used during powder production.

Further, the produced powder particles are completely different between the gas atomization and water atomization. Figure 5a, b show the variations in powder morphology of stainless powders obtained from gas atomization and water atomization respectively. The gas atomization method has produced a spherical shape powder particle (Fig. 5a) in the range between 3 µm and 40 µm with the average particle size of 20 µm. On the other hand, the same stainless steel material has possessed irregular powder particle shape (Fig. 5b) through a water atomization technique. The particle sizes

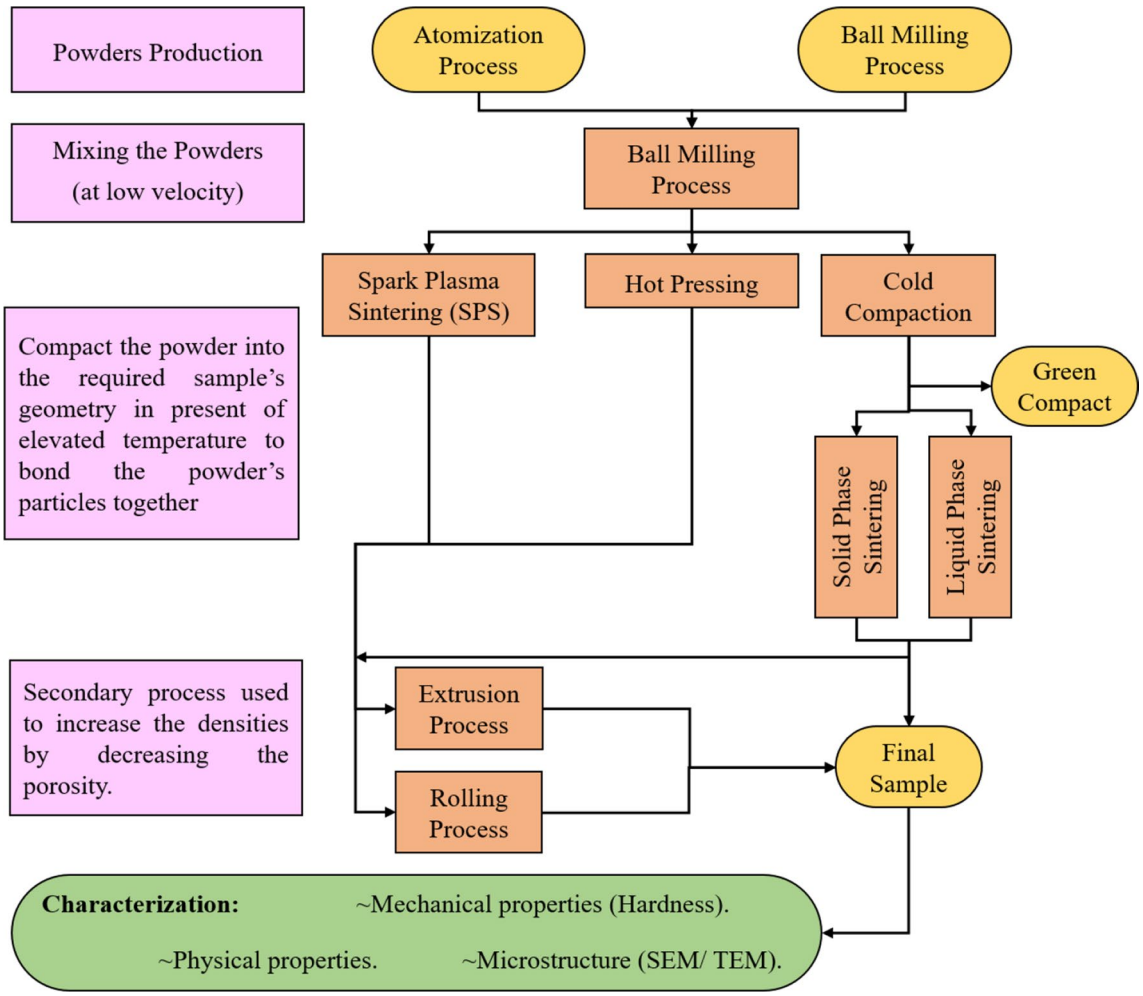

Fig. 3 Schematic of solid-state processing routes for HEAs

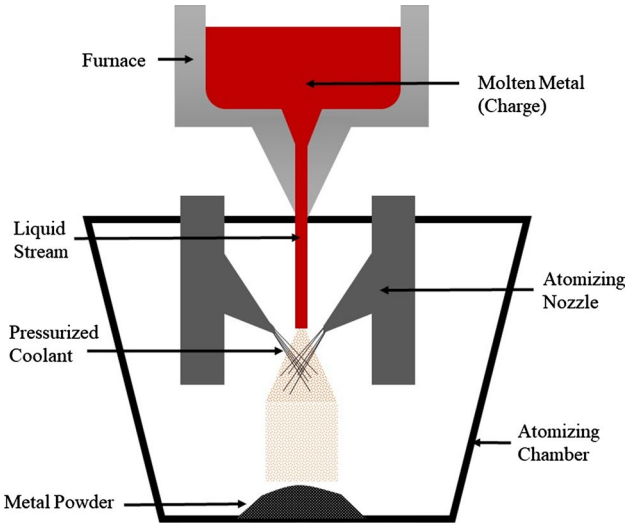

Fig. 4 Schematic of the working principle of the powder atomization process

Table 1 Recommended power atomization process variables range [32]

Gas pressure	1.4–42 MPa
Gas velocity	50–150 m/s
Superheat	373–473 K
The angle of impingement	15–90°

are in the range from 6 µm to 50 µm with the average particle size was 30 µm [33]. Recently, Yang et al. [34] have synthesized AlCoCrCuFeNiSi HEA through the gas atomization process which the obtained powders exhibited spherical shape with a smooth surface. This spherical shape with smooth surface powder particles can be used as raw powders for AMT. Similarly, Zhoui et al. [35] have also produced $Al_{0.6}$CoCrFeNi HEA powders with spherical shape (Fig. 5c). In contrast, Yim et al. [36] synthesized CoCrFeMnNi HEA powders by water atomization technique which showed that few powder particles were spherical and most of the powders particles were flat and potato in shape (Fig. 5d). These big shape changes in the powder morphology can influence the physical and mechanical properties much. It is well known that the thermal carrying capacity of the gas cooling medium is low when compared to the liquid cooling medium. Due to this, the alloy powders obtained from gas atomization get cooled slowly which provides more time to shrink during the fall of the powder particles which yield sphere shape. Liu et al. [37] investigated a single FCC phase of CoCrFeMnNi HEA processed by gas atomization and MA. The results were revealed that this HEA produced good mechanical properties (tensile strength of ~ 1.0 GPa, ductility of ~ 6%), and nanocrystalline structures when compared to the gas atomized route. More addition, Wang et al. [38] have synthesized a single-phase non-equiatomic $CrFeCoNiMo_{0.2}$ HEA (FCC phase) which was tested its mechanical behavior at different temperatures (600–1100 °C) and strain rates (10^{-3}–10^{-1} s^{-1}). The incorporated Mo addition yielded more activation energy, lattice distortion, and grain refinement due to which useful enhanced mechanical properties were obtained.

2.2 High Energy Ball Milling Method (HEBM)

The ball milling is a horizontal and cylindrical machine mostly utilize in grinding all types of metals and ceramics. Figure 6 shows the schematic of the conventional ball milling technique which usually consists of slow speed rotating drum, and grinding balls which are made of hardened stainless steel or titania, or ceramics. The materials (medium) which are to be ground, partially fills the cylindrical jar with an appropriate media to medium ratio. In industrial scale, the ball milling runs for days by feeding the device from one end, then discharges the powder form in another end after reducing larger unit masses to smaller unit masses (size reduction process). The commercial horizontal type ball mills (Fig. 6) can be used to manufacture homogeneous alloy on an industrial scale. However, these mills cannot be used to synthesize the nanostructured materials and HEA powders. HEBM method can be used to synthesize the nanostructured HEAs powder.

Planetary ball mill is an advanced version of common ball milling in which vertical grinding jar(s) is/are attached to horizontal disk called sun wheel or planetary disk as demonstrated in Fig. 7. The rotation of the direction of the jar is reverse to the direction of the sun wheel with a standard velocity ratio of the sun wheel to the jar are 1:1, 1:2, and 1:3. The advantage of planetary ball milling is to produce a nanostructured homogeneous powder particle (nano-scale particle). Some studies have reported that the use of conventional ball milling and the HEBM capable of producing the powders, decreasing the particle size and mixing the powders among each elemental constituents. Most certainly, the revolution velocity is different from one study to another, but all the studies agreed that a slower velocity is used for mixing the powders than a high velocity which can be used to reduce the crystallite/grains/powder particle sizes. One of the common limitations of this process under dry milling is an agglomeration of powder particles due to more surface energy in the powder particles. Fortunately, nowadays, the formation of agglomerations can be minimized either via mechanical alloying (MA) [39] or by mechanical milling process (both dry and wet milling) by adding process control agent (PCA). Certain weight percentage of stearic acid and or other organic compounds (NaCl, Na_2SO_4, KCl etc…) with the powders are being added during the ball milling process as PCA [27, 40, 41]. Very high configurational entropy alloys can be easily produced via HEBM

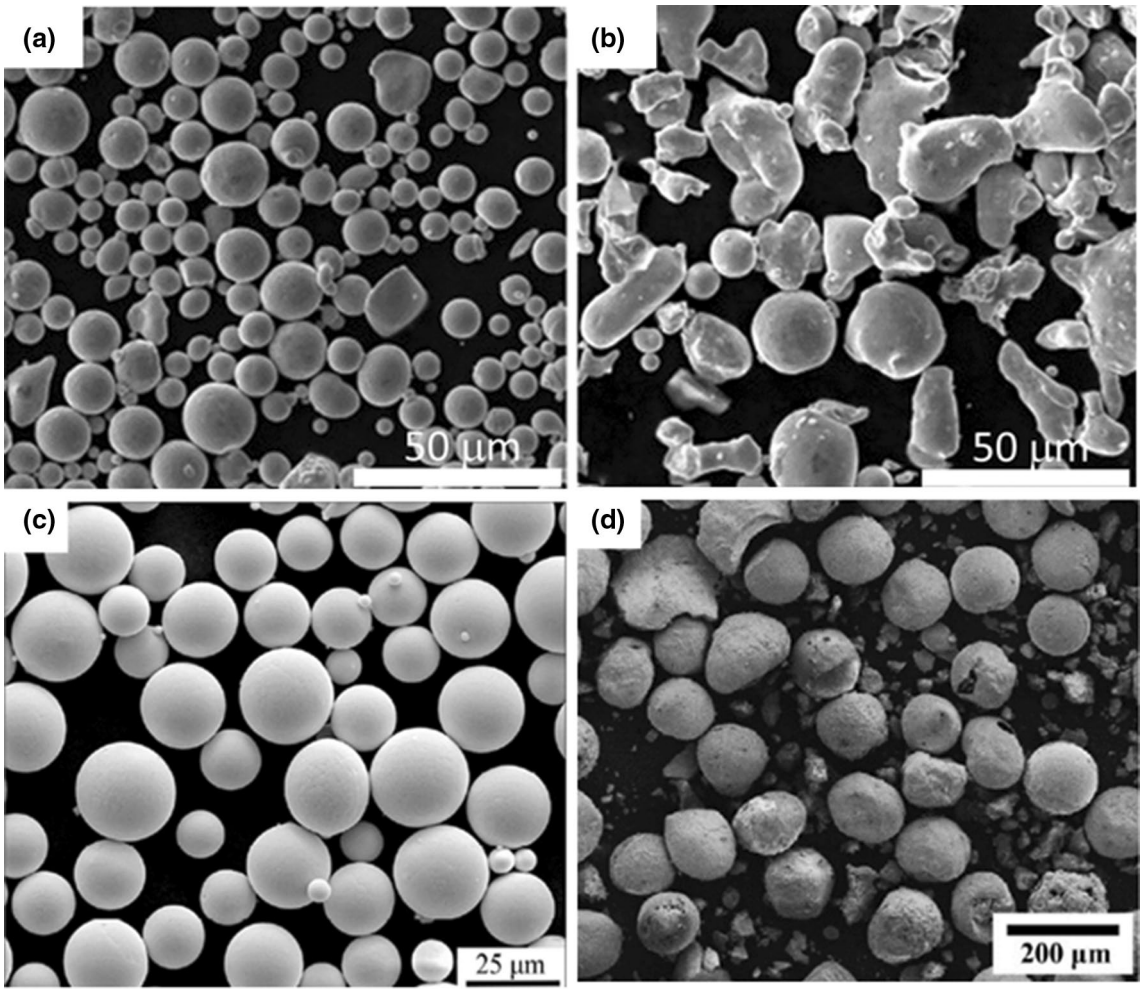

Fig. 5 SEM powder morphology of: stainless steel powder produced by: **a** gas atomization; **b** water atomization [33]; **c** Al0.6CoCrFeNi HEA powder by gas atomization [35]; **d** CoCrFeMnNi HEA powder by water atomization [36]

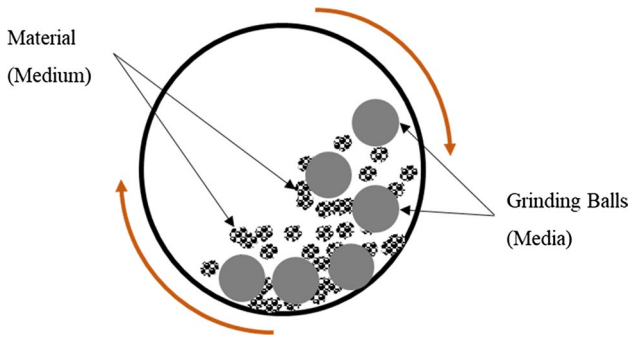

Fig. 6 Schematic of conventional ball Milling Device

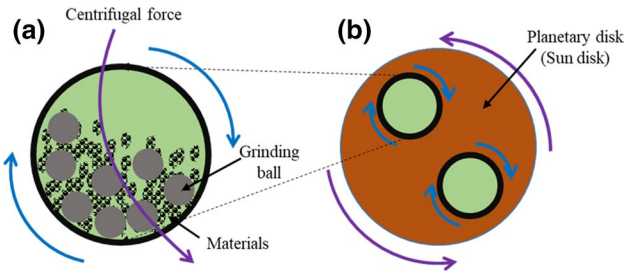

Fig. 7 **a** Grinding jar; **b** high-energy ball milling (HEBM)

from the mixing of pure elemental powders without forming any intermetallic phases. In addition, HEBM can be used to manufacture high-melting alloys which are difficult by casting route/liquid metallurgy route. Cheng et al. [42] synthesized CoCrNiMnAlx (x = 0, 0.1, 0.3, 0.5, 0.7, 1) HEAs through MA with BPR of 15:1, speed of 250 rpm, and milling time of 45 h. From XRD results, Fig. 8a, the formation of alloying was confirmed. XRD patterns indicate a stable FCC phase when the Al concentration was less than 0.5. With the increasing of Al concentration of more than 0.5, the FCC phase was destabilized and increases the BCC phase formation. These results were attributed to the large atomic

radius value of Al atoms which dissolved into BCC lattice. Further, nanostructured CoCrNiMnAlx HEAs and the phase formations were confirmed by TEM (Fig. 8b, c). Oleszak et al. [43] have synthesized WMoNbZrV HEAs which possessed high-melting point. It was found that the produced high-configurational entropy powders (50 h) were retained its crystallite size of 10 nm and BCC crystalline structure until 700 °C which ensured the attainment of high thermal stability. Yurkova et al. [44] have synthesized AlCuNiFeCr HEA by MA/HEBM who has achieved super saturated SS with a stable BCC crystal structure. The amount of solid solubility, alloy formation, crystal size reduction, structural changes etc.… mainly depends on several HEBM parameters. Emamifar et al. [45], investigated the effect of milling time on AlCrFeCoC HEA in which the results explained that the particle size and shape of HEA powders were strongly influenced by the function of milling time. However, the commonly used HEBM parameters for manufacturing the nanostructured HEAs are illustrated in Table 2. Unfortunately, this process utilizes in research purposes and laboratories only. Contamination is the main drawback in HEBM due to a small amount of HEA powders production which directly affects the final properties.

2.3 Cold Uniaxial Pressing Method

A cold pressing (CP) process is the one which includes the step of powders production, and consolidation of powders by compressing the powder particles together into the one-piece called green compact via a pressing tool at room temperature (Fig. 9). During cold uniaxial pressing, the prepared powder particles are to be filled inside the die (usually made of tool steel, H13 steel, EN steel) which is usually placed between two punches (Bottom one and top one). Look after, the punches can start to press the powder particles which is called uniaxial compaction as the direction of load is in one direction. This CP process is a simple and economical one as it is still being used in the mass production industries. Yuhu et al. [47] have consolidated the $AlNiCrFe_xMo_{0.2}CoCu$ HEA powder by the uniaxial pressing process (compacted at 310 MPa) and achieved the relative density of more than 91% after sintering. Shivam et al. [48] have also consolidated the AlCoCrFeNi HEA powder by CP method (625 MPa). Baldenebro-Lopez et al. [49] manufactured AlCoFeMoNiTi HEAs via two routes to examine the influence of processing methods: (1) MA (10 h, BPR of 5:1), uniaxial pressing (1.5 GPa) and vacuum sintering (VS, 1424 K for 3 h), (2) MA, uniaxial pressing and arc melting (AM). The results were explained that the SSP of MA, uniaxial pressing, and VS have produced improved microstructures and mechanical

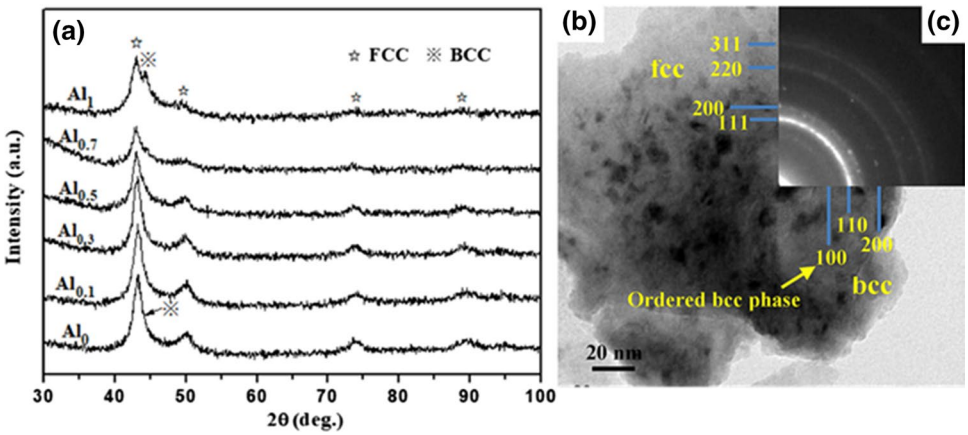

Fig. 8 **a** XRD patterns of CoCrNiMnAlx (x = 0, 0.1, 0.3, 0.5, 0.7, 1) HEAs prepared by MA after 45 h; **b** TEM bright field image of $CoCrNiMnAl_0$ HEA showing FCC and BCC phases; **c** SAED pattern on **b** [42]

Table 2 Generally used HEBM parameters during the synthesis of nanostructured materials [46]

Ball-to-powder ratio (BPR)	5:1, 10:1, 15:1, 20:1
Sun wheel speed, rpm	50, 75, 100, 150
Planet vial speed, rpm	150, 225, 300, 450
Milling time, h	1, 5, 10, 15, 20, 25, 30, 40, 50, 60, 80, 100
Process control agent (PCA), to avoid agglomeration	Steric acid, ethanol, gasoline, toluene etc…
Milling forward: pause: milling reverse time (depends on the elemental composition)	10:10:10; 15:15:15, 20:20:20
Milling medium	Hardened stainless steel, tungsten carbides
Ball diameter, mm	6, 8, 10, 12, 15
Distribution of size of balls	Uniform size, non-uniform size

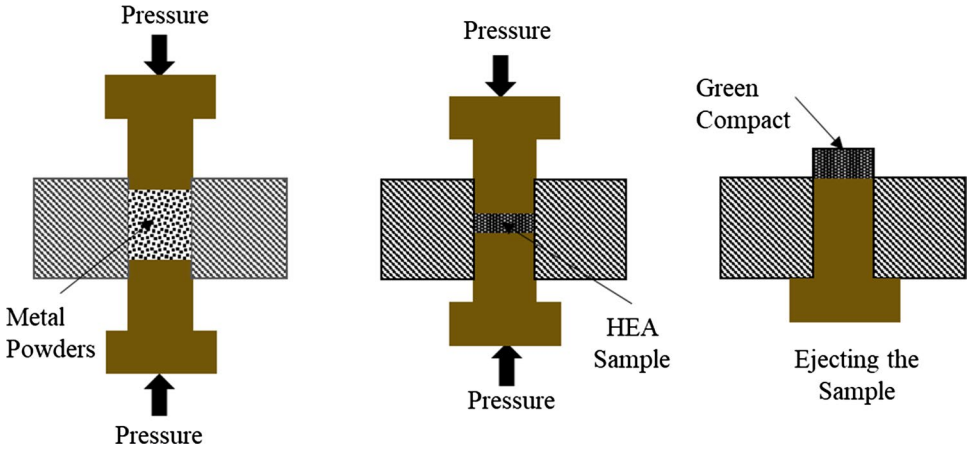

Fig. 9 Schematic of cold pressing (CP) process

properties (Fig. 10). There was no porosity in the former method when compared to AM method. This result indicates that the processing route influences the properties (Vickers hardness strength (VHS): 8.8 GPa for VS sample, 7.85 GPa for AM sample) and microstructures significantly. However, the cold uniaxial pressing process produces non-uniform densification when the aspect ratio of the sample exceeds or near to 1.

2.4 Sintering Process

Sintering is a densification process where the powder particles are compacted and formed via applying heat below the melting point or liquefaction point [41] under the inert gas atmosphere. The purpose of this process is to bond all the powders together so the mechanical and physical properties can be improved. The schematic of the sintering process in the different stages is shown in Fig. 11. There are two types of sintering, namely, solid-phase sintering, and liquid phase sintering (LPS). The LPS is commonly used in materials that are hard to sinter. In solid-phase sintering, particle-to-particle diffusion bonding can be carried out. Usually, vacuum hot pressing (VHP) sintering and spark plasma sintering (SPS) are the commonly used consolidating techniques for HEA powders. In HEAs, the LPS is not recommended because of changes in the microstructural phases [50]. Sintering process can be divided into three sections which are: (1) heating (increase the temperature rate, (2) holding (fix the temperature for certain time) and (3) cooling (decrease the temperature rate). Xu et al. [51] prepared a ternary alloy of $FeMn_{28}Six$ (x = 0, 1, 2, 3, 4 wt%) alloy through HEBM of powder metallurgy (PM) routes. The elemental powders were ball milled using HEBM (BPR of 5:1, 275 rpm, 4 h), compacted using the uniaxial compaction method (400 MPa) followed by sintering the green compacts under vacuum (5×10^{-3} Pa). The sintering cycle used was heating the green compact from room temperature to 1073 K with a heating rate of 10 °C/min, hold at 1073 K for 1 h, then again heated the samples to 1473 K with a heating rate of 5 °C/min, hold it for 3 h, and finally cooled the samples inside the furnace itself. The Fe–28Mn–4Si sample exhibited the UTS of around 350 MPa. These results indicated that ternary HEAs can be manufactured using conventional sintering under protective environmental conditions.

2.5 Hot Pressing Process

Hot pressing (HP) process is a combination of both CP and sintering process which is simultaneously carried out. The advantage of this process is increasing the density of the

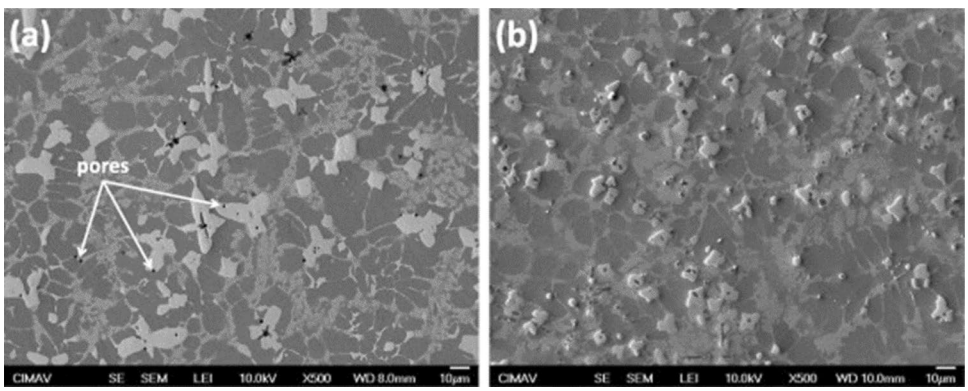

Fig. 10 SEM images of AlCoFeMoNiTi HEAs prepared by: **a** as-cast by arc melting process; **b** uni-axial pressing followed by vacuum sintering (Baldenebro-Lopez et al. [49])

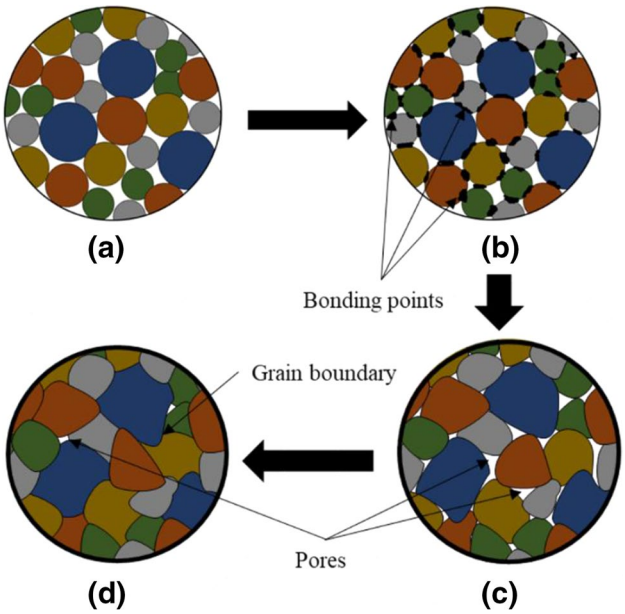

Fig. 11 The schematic of sintering stages: **a** bonding points in green compact at particles attached with each other; **b** necks formed from bonding points; **c** reduction in size of the pores between grain boundaries; and **d** grain boundaries grow between particles

product and reducing the porosities. In HP process, the axial load is applied on the heated powders inside the die as illustrated in Figure 12a. This HP can be carried out under vacuum or room temperature. HP can be used to consolidate the HEA powders into the bulk form [50]. Fu et al. [52] have consolidated $Al_{0.6}NiFeCrCo$ and $Al_{0.6}NiFeCr$ HEAs under the VHP process. The used VHP process parameters were vacuum pressure of 1.2×10^{-2} Pa, uniaxial applied pressure of 30 MPa, at a temperature of 1000 °C for 1 h. Sun et al. [50] have consolidated $Fe_{18}Ni_{23}Co_{25}Cr_{21}Mo_8WNb_3C_2$ HEA using HP at different temperatures (400, 600 and 1050 °C for 2 h). HP was carried out at 30 MPa pressure under a vacuum. An ultimate tensile strength (UTS) of around 1.45 GPa with 4% ductility was obtained whereas a UTS of 0.8 GPa with 13.3% was obtained at a high temperature of 650 °C. These high-temperature mechanical properties are very much useful in structural applications. Hence, this HEA can be used in the place of well-known super alloys (GH1040, A286, and K2135). The formation of intermetallic phase(s), and more consolidation time are the main drawback of this HP process. For instance, the second phase precipitates of eta-phase carbides (M_6C) formation in HPed HEA is shown in Figure 12b (HEA of $Fe_{18}Ni_{23}Co_{25}Cr_{21}Mo_8WNb_3C_2$, [50]). Also, in the upgraded process of HP, an isostatic pressure is being used which is called hot isostatic pressing (HIP, Fig. 13a). Figure 13a shows the schematic of HIP process in which the materials to be consolidated are put inside a metal canister (usual steel), then filled canister is placed inside the controlled hot chamber, and finally, the materials are to be pressed with iso-static pressure (360° direction) under inert medium. Due to which high-density products can be obtained. Tang et al. [53] consolidated AlCoCrFeNi HEA through HIP, investigated the tensile properties and finally compared the same HEA in the as-cast condition. This HEA was synthesized via VAM method followed by consolidation of the as-cast HEA using HIP at 1273 k under 207 MPa for 1 h. The phase-map microstructure of as-cast and HIPed AlCoCrFeNi HEA is shown in Fig. 13b, c respectively. Nonhomogeneous dendrites with porosity were obtained in as-cast alloy (Fig. 13b) whereas homogeneous microstructure was obtained in HIPed alloy (Fig. 13c. The UTS of as-cast HEA produced around 400 MPa with the ductility of 1% whereas the HIPed HEA sample exhibited the UTS of 393 MPa with the ductility of ~ 12%. This is due to homogeneous heat treatment by HIP which changed the microstructures completely. From this, it can be understood that an improved mechanical property from HEAs can be obtained through HIP process. However, as a consequence of the large surface area of loose powders, the oxidation of HEA powder at elevated temperature increases. Also, this technique required more complex and expensive systems such as heating, pressure, and vacuum systems than conventional cold pressing followed by sintering [54].

Fu et al. [55] investigated the sintering behavior of $Al_{0.6}NiFeCrCo$ and $Al_{0.6}NiFeCr$ HEAs prepared by MA

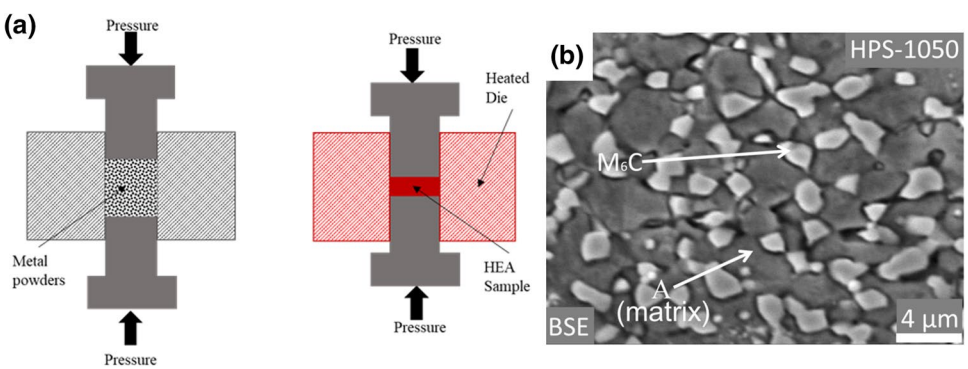

Fig. 12 **a** Schematic of hot pressing (HP) process; **b** SEM image of HPed 1050 ($Fe_{18}Ni_{23}Co_{25}Cr_{21}Mo_8WNb_3C_2$, [50]) HEA

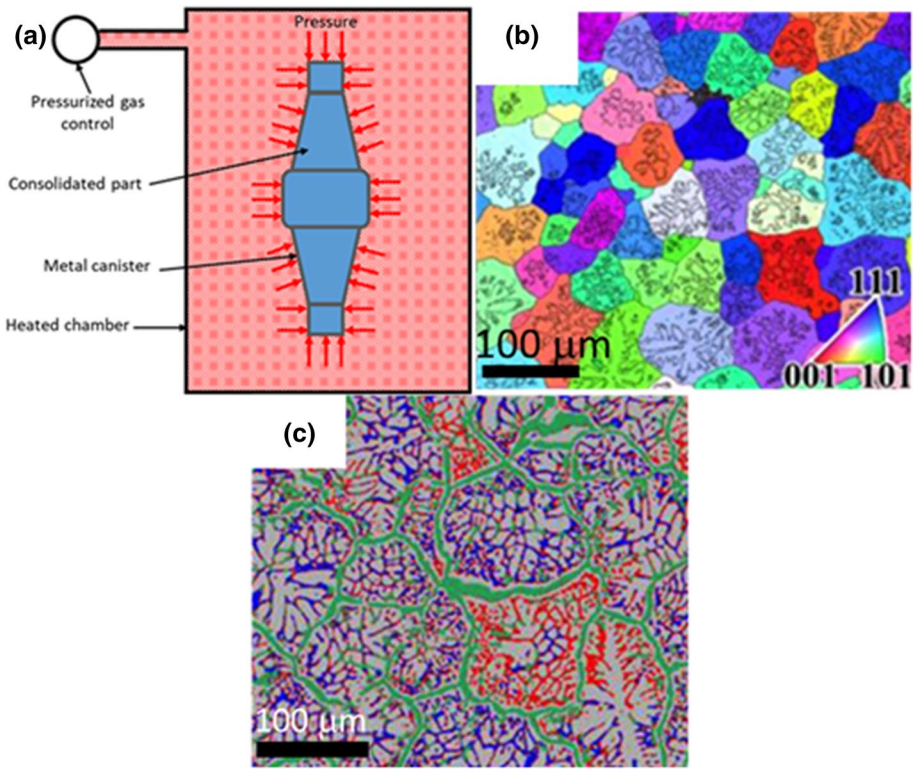

Fig. 13 **a** Schematic of hot isostatic pressing (HIPing) process; **b** Phase map microstructure of as-cast AlCoCrFeNi HEA; **c** As-HIPed AlCoCrFeNi HEA [53]

and consolidated by HP. These HEAs were produced 85% BCC and 15% FCC SS phases in powder state condition. However, these two HEAs were exhibited 69% FCC and 31% BCC phases after HP with good mechanical properties (density, hardness, and mechanical strength).

2.6 Spark Plasma Sintering

SPS is a novel sintering technique and is well known as pulsed electric current sintering (PECS) or pressure-assisted pulse energizing process. This technique is mostly used to densify powders in a faster manner due to its effective and remarkable features, namely, energy conservation and fewer procedure steps when compared to the conventional sintering techniques. Further, a homogeneous bulk single SS alloy can be retained after processing with improved microstructural features and mechanical properties. The principle idea of SPS is that the pressure ram which is work as electrode attached to direct current (DC) source as shown in Fig. 14. The DC is infiltrated (750–1500 A) through the powders by the graphite punch simultaneously the powder particles are being compressed (25–150 MPa). Using SPS, very high dense products with nanostructures and limited grain growth can be achieved based on desired sintering parameters. Eißmann et al. [56] have consolidated CoCrFeMnNi HEA at 1000 °C using SPS and achieved a high dense structure (> 98%). From the SEM image of Fig. 15a, it was very clear that there was a single-phase formation without any abnormal precipitates. The variation of the grey region indicates the different grain directions; which is not a different phase. The XRD patterns of Fig. 15b confirm a single FCC phase formation which explains that there was no intermetallic phase formation through SPS. Here, CoCrFeMnNi HEA produces a single FCC phase in both synthesized and consolidated conditions. Yurkova et al. [44] have consolidated AlCuNiFeCr HEA using SPS which was prepared by MA. The authors were reported that the produced HEA powders were sintered using SPS with different temperatures (700, 800, and 900 °C) at 150 MPa. After SPS, the HEA sample was exhibited around 75% ordered BCC SS, and 25% FCC SS. Fu et al. [52] have synthesized a HEA of $Co_{25}Ni_{25}Fe_{25}Al_{7.5}Cu_{17.5}$ through MA followed by SPS in which an average grain size of 90 nm was achieved after SPS. Pan et al. [57] manufactured refractory based HEAs of $Nb_{25}Mo_{25}Ta_{25}W_{25}$ and $Ti_8Nb_{23}Mo_{23}Ta_{23}W_{23}$ via MA and SPS. The authors have achieved a single stabilized BCC structure with ultra-fine grains (UFG) after SPS. Recently, Yim et al. [58] have synthesized CoCrFeMnNi HEA reinforced with TiC composite by water atomization, MA and SPS (50 MPa, 950 °C) methods. Emamifar et al. [45] have sintered the $Al_{0.5}CrFeNiCo_{0.3}C_{0.2}$ HEA using SPS (35 MPa, 1000 °C) and reported that the hardness of sintered HEA was increased drastically with the function of milling time (5, 10, 27, 35, 45 h). Based on this, it is very clear that the MA process followed by SPS can be used to synthesis the nanostructured HEAs effectively. But the SPS is limited due

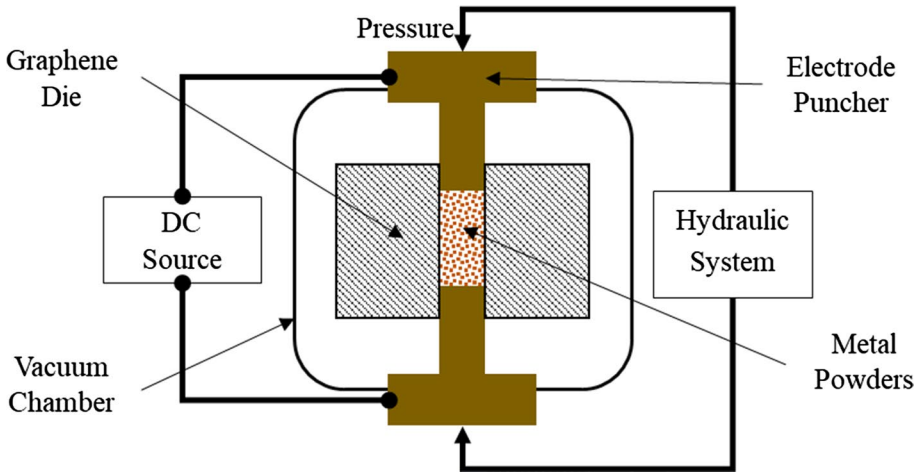

Fig. 14 Schematic of the working principle of spark plasma sintering (SPS) process

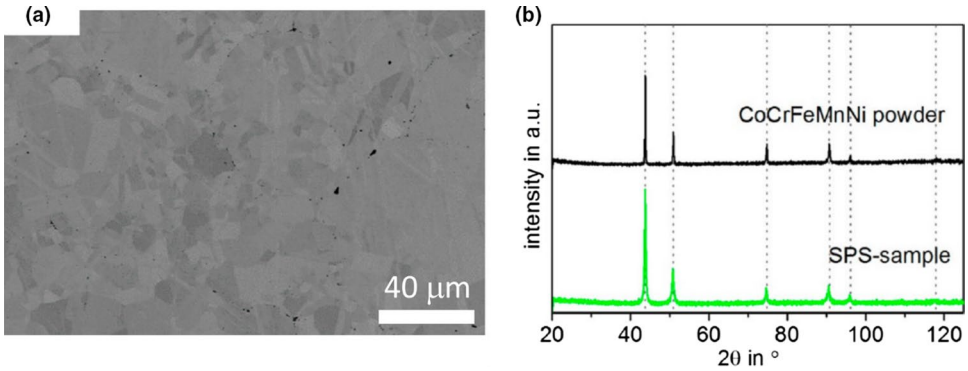

Fig. 15 **a** SEM image of spark plasma sintered CoCrFeMnNi HEA; **b** corresponding XRD patterns for as-milled powder and after SPS [56]

to symmetrical shape required for the sample and also SPS needs pulsed DC source.

Mohanty et al. [59] investigated the aging behavior of $Al_{20}Co_{20}Cu_{20}Ni_{20}Zn_{20}$ HEA which was prepared by MA followed by SPS at 950 °C. The sintered sample produces FCC (β) SS primary phase and L12 (α) secondary phase. This sintered HEA was heated at 1160 °C, hold it for 96 h, and then solution treated. The solution treated HEAs were then aged at different temperatures (400 °C, 500 °C, 600 °C, 800 °C, and 1000 °C) withholding time of 48 h. Aged HEA samples produced L12-α and FCC-γ phase. The results explained that the sample aged 500 °C exhibited a high hardness value of around 6.25 GPa which was due to the combination of several strengthening mechanisms (see "Appendix of ESM"). Zhang et al. [60] examined the various phase evolutions in CoCrFeNiTiAl HEA processed by MA and consolidated it by SPS. This HEA has produced a supersaturated FCC and BCC solution phases in as-milled conditions with an average crystallite size of 40 nm. However, the same HEA has produced two major BCC phases and a minor FCC phase after SPS followed by annealed at 600 °C for 1 h. Further, this HEA has exhibited a relative density of more than 98% and VHS of 4.35 GPa. In HEAs, grain refinement is also possible by adding some elements by which the mechanical properties can be increased extensively. For instance, Pan et al. [57] synthesized two HEAs which are $Nb_{25}Mo_{25}Ta_{25}W_{25}$ and $Ti_8Nb_{23}Mo_{23}Ta_{23}W_{23}$ in which Ti was added as a grain refiner through MA followed by SPS. The electron backscattered diffraction (EBSD) SEM images were confirmed the refinement of NbMoTaW matrix grains and the same is shown in Fig. 16. Further, these two HEAs produce BCC primary phase and BCC precipitates (B2) which is also shown in Fig. 17 (TEM images). Ganji et al. [61] have synthesized AlCoCrCuFeNi HEA prepared by MA followed by SPS at 750 °C. Complete single-phase SS of FCC phase was achieved in as-milled powders whereas an FCC and ordered BCC (B2) phases were obtained after SPS which has bimodal grains (Fig. 18). This HEA has exhibited around 8 GPa VHS and 170 GPa modulus of elasticity. Now, from these microstructural evolutions, due to the presence of SS phases, HEAs produce extensive properties improvement when compared to conventional materials. Fu et al. [52] investigated non-equiatomic FCC $Co_{25}Ni_{25}Fe_{25}Al_{7.5}Cu_{17.5}$ HEAs processed by PM route (MA and SPS) and casting route. The results explained that around 1.8 GPa YS and 4.6 GPa VHS were obtained in HEA via PM route which was 835% high in YS and 252% more in hardness when compared to cast one. These improved results were due to

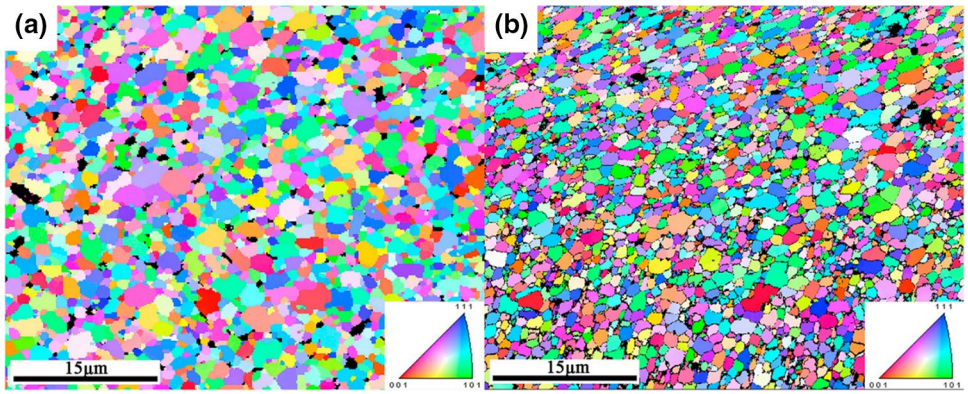

Fig. 16 Grain refinement—effect of Ti addition in HEAs-EBSD images on bulk HEAs samples consolidated by SPS at 1600 °C: **a** $Nb_{25}Mo_{25}Ta_{25}W_{25}$, **b** $Ti_8Nb_{23}Mo_{23}Ta_{23}W_{23}$ [57]

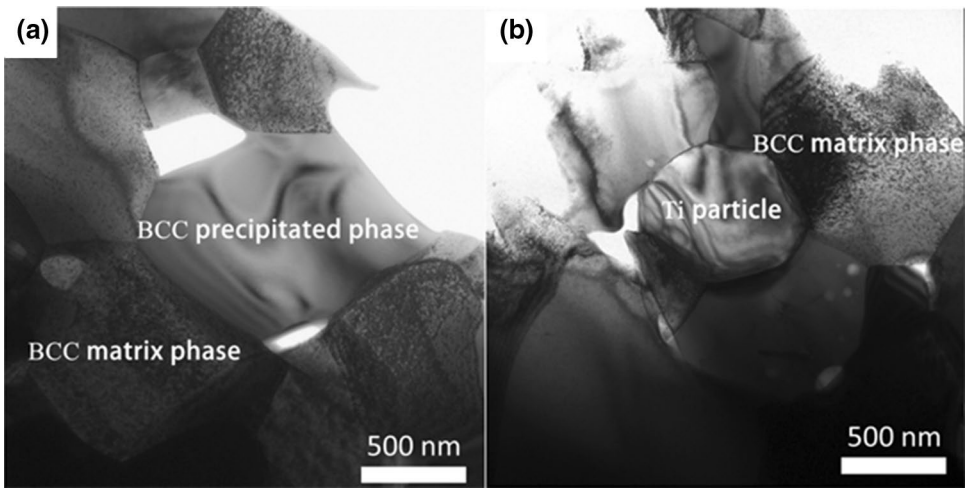

Fig. 17 TEM micrographs showing BCC primary matrix phase and BCC precipitates (B2 phase) in HEAs consolidated by SPS at 1600 °C: **a** $Nb_{25}Mo_{25}Ta_{25}W_{25}$, **b** $Ti_8Nb_{23}Mo_{23}Ta_{23}W_{23}$ [57]

grain boundary strengthening and dislocation strengthening mechanisms (see appendix).

3 Liquid State Processing Methods

HEAs can also be manufactured through the melting and casting technique in which VAM (for HEAs) and mechanical stirring (MS, for HEA based composite) are the common processing methods. In addition, liquid infiltration techniques can also be used for the manufacturing of HEAs. Figure 19 shows the schematic of LSP methods to synthesis HEAs. The main drawback of the LSP method is the evaporation of low melting elements. It can be controlled by resistance heating and induction heating furnaces. The formation of heterogeneous microstructure due to the slow rate of solidification is another disadvantage in the casting route for HEAs. Several researchers have successfully manufactured HEAs through LSP methods [62–66].

3.1 Arc melting Process

Many scientific studies have succeeded to produce HEAs with significant physical, chemical, and mechanical properties by using the AM process [10, 30, 66]. The low energy consumption, time-saving, and lower amount of porosity are the main advantages of AM process and hence, scientists and researchers have focused to manufacture HEAs using this AM process. Figure 20 shows the AM process where the alloy ingots or alloy powders were put on metallic crucibles and melt them by tungsten electric arc which struck under inert gas (argon atmosphere) after vacuum the chamber to avoid any oxidation. The alloy ingots or powders repetitively melted by the AM and solidified by the coolant which is located beneath the metallic crucible several times to ensure the homogeneity of the alloy. Otto et al. [65] have investigated an equiatomic CoCrFeMnNi HEA processed by AM and casting processes. The microstructural evolutions and mechanical properties were investigated during room temperature deformation. This HEA has produced VHS 4.2 GPa. Novak et al. [67] have examined the influence of Mn

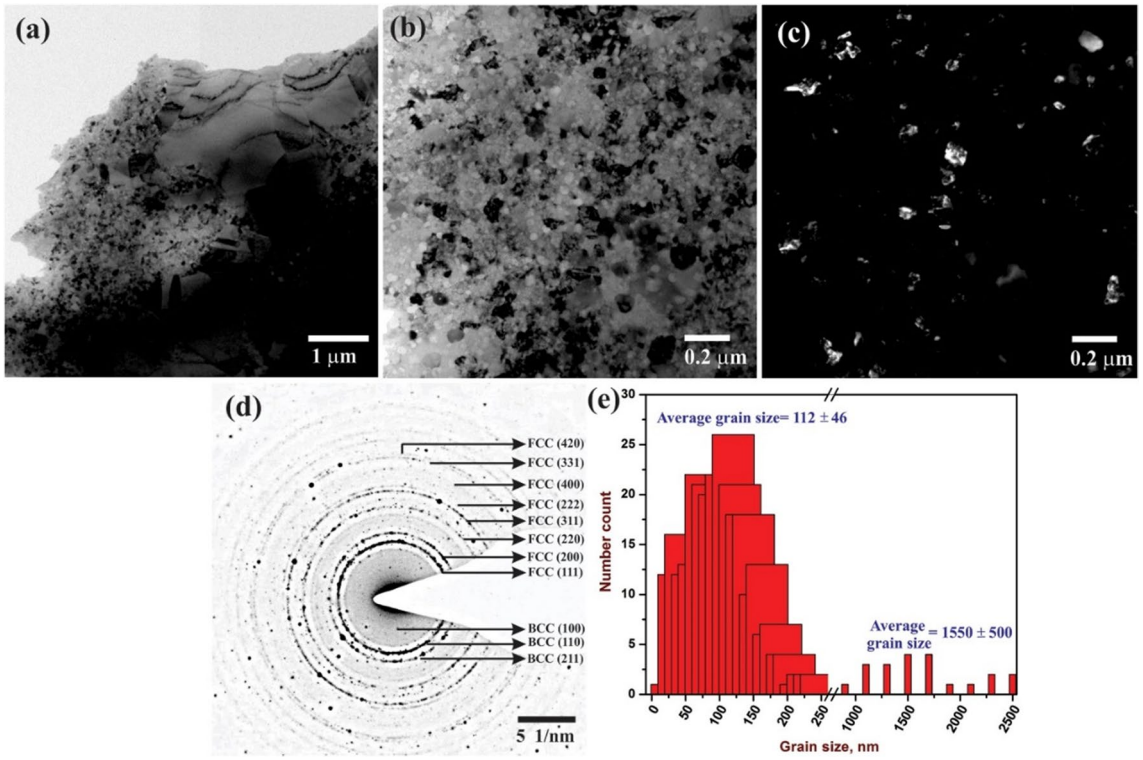

Fig. 18 TEM images of AlCoCrCuFeNi HEA after SPS at 750 °C: **a** bright-field image (BF); **b** BF image at high magnification of **a**; **c** dark field image; **d** SAED pattern showing FCC and BCC phases; **e** grain size distribution. [61]

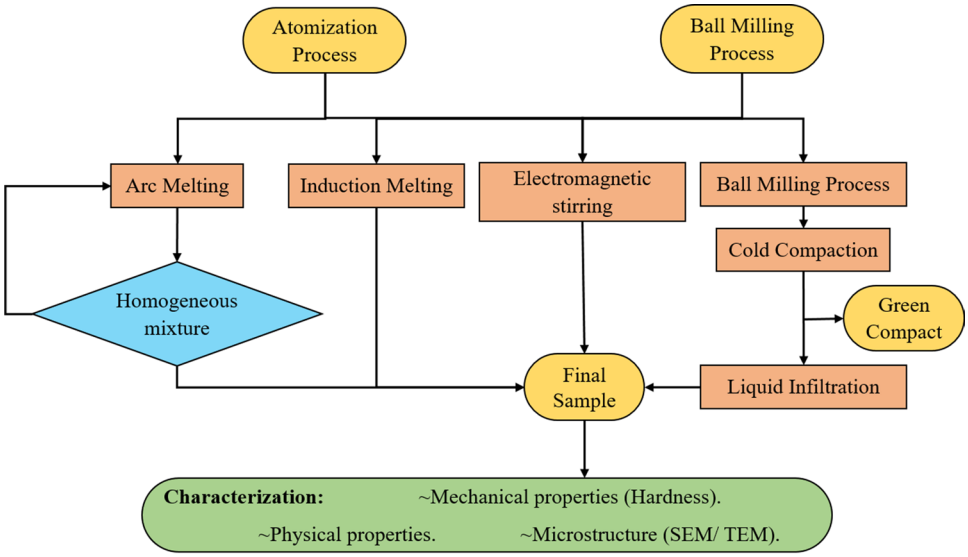

Fig. 19 Schematic showing various processing methods in liquid metallurgy route for HEAs

incorporation in AlCoCrFeNi HEA processed by laser melting. The observed microstructures were produced major FCC phases and some precipitates. This result has explained the addition of Mn in AlCoCrFeNi HEA led to producing a single FCC crystal structure. Hou et al. [68] have investigated microstructures and mechanical properties of AlFeCoNiBx (x = 0, 0.05, 0.10, 0.15, 0.2) HEAs prepared by VAM method. The results were revealed that the incorporation of boron content in the AlFeCoNi matrix led to converting BCC phase to BCC and FCC phases. With higher value of boron content, the AlFeCoNix (x = 0.15, 0.2) matrix of HEAs produces eutectic phases ($BCC + FCC_1 + FCC_2$). In addition, the observed microstructure was pure BCC phase when there was no boron.

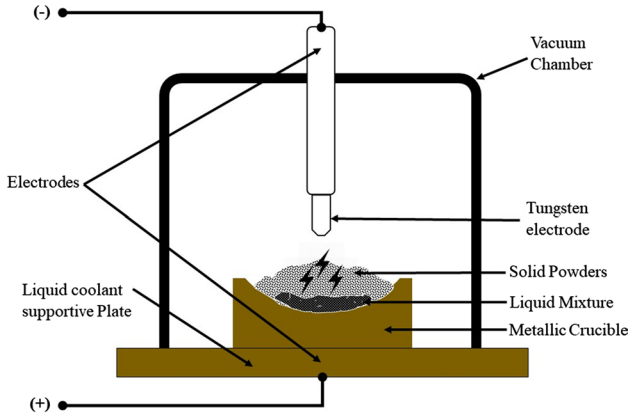

Fig. 20 A descriptive diagram of the arc melting method

However, the dendrite and eutectic phases were formed with increasing of boron content. The same microstructural observation is shown in Fig. 21.

3.2 Vacuum Induction Melting Process

It is a process of heating electrical conducting materials through electromagnetic induction causing a magnetic field. This magnetic field permeates the electrical current over the conducting materials consequently it generates an electrical current called Eddy current; which then is used to heat the materials. The ingot located inside the crucible furnace prevents the input current consequently the magnetic field generates through electrical conducting materials which melt them rapidly from inside as shown in Fig. 22. Then, cooling down the ingot and re-melt several times to get homogenous HEA [15, 69–72]. At the final melting stage, the molten state of HEAs is to be poured into the desired mold and allowed it for solidification. This melting of HEAs has to be carried out under a high vacuum. Qiu et al. [73] have investigated the influence of Fe content in $Fe_xCoNiCu$ (x = 1.5, 2, 2.5, 3) HEAs in which the raw materials (Fe, Co, Ni, Cu in the form of blocks) have put inside the graphite crucible for VIM. The melted HEAs were poured into a copper mold which was then cooled to room temperature. The obtained results have explained that the increasing of Fe content in FeCoNiCu HEA matrix has shifted the formed microstructure from FCC phase ($Fe_{1.5}CoNiCu$) into the combination of both FCC and BCC phases ($Fe_{2.5}CoNiCu$). The highly incorporated Fe content based HEA ($Fe_{2.5}CoNiCu$) produced a VHS of 6.72 GPa which was 2.21 times higher compared to $Fe_{1.5}CoNiCu$ HEA due to more amount of BCC phase. Besides, the UTS of $Fe_{2.5}CoNiCu$ HEA has exhibited 639 MPa which was 110% more compared to $Fe_{1.5}CoNiCu$ HEA. Kim et al. [74] have also studied the microstructural evolutions and mechanical properties of $Co_{10}Cu_{20}Mn_{30}Ni_{40}$ HEA produced by VIM. The casting was carried out under argon atmosphere; the raw materials in the form of elemental

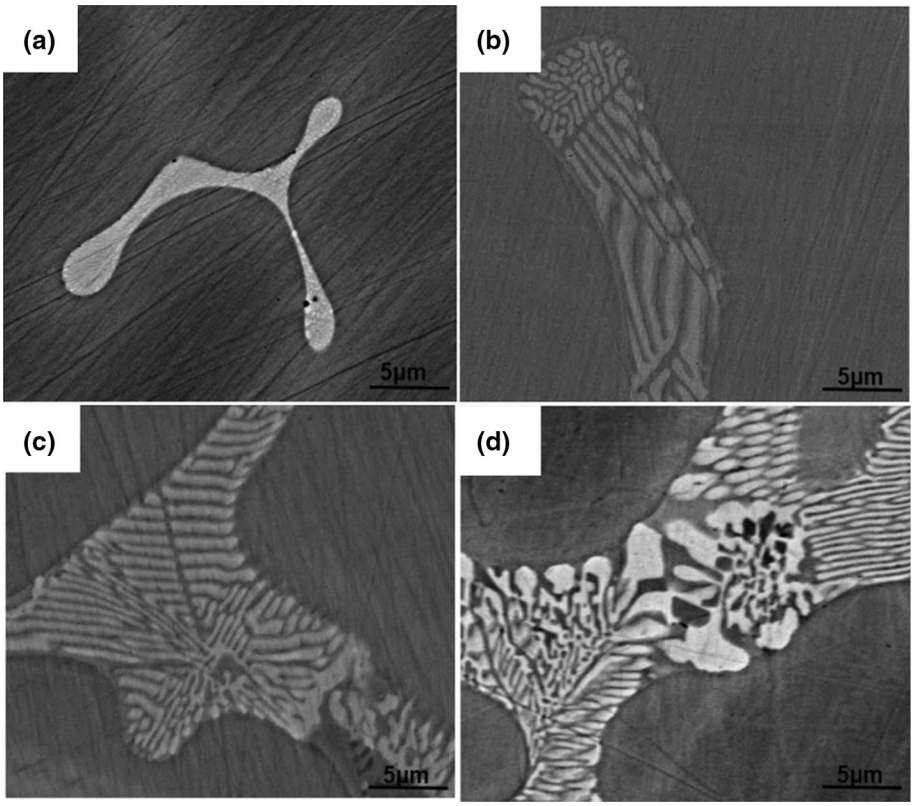

Fig. 21 SEM images of as-cast AlFeCoNiBx alloys by vacuum arc melting method: **a** x = 0.05; **b** x = 0.10; **c** x = 0.15; **d** x = 0.20 (Hou et al. [68])

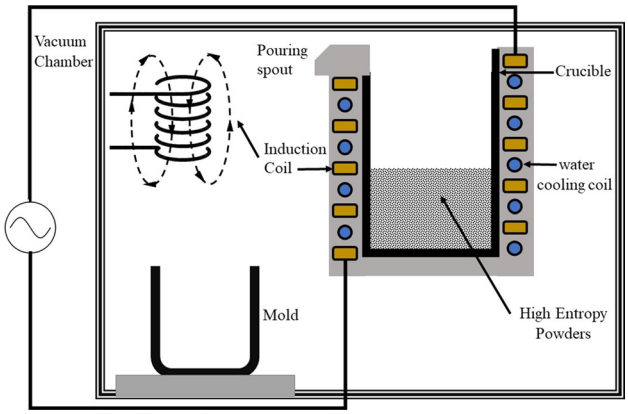

Fig. 22 Schematic diagram of the vacuum induction melting process

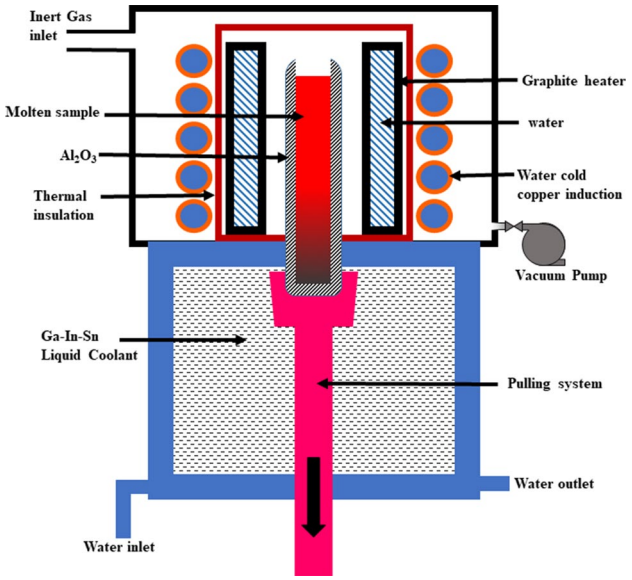

Fig. 23 Schematic of directional solidification process

powders were added in the alumina crucible to get master alloy; then the graphite crucible was used to have a homogenized alloy at 1373 k for 6 h; the homogenized cast ingot was rolled to thick sheet (1.5 mm) with a reduction ratio of 75%; and finally the rolled sheets were heated at different temperatures (873, 923, 1023, 1073, and 1173 K). The results were explained that a fully re-crystallized stable FCC phase with 2.8 mm refined grains were obtained in the HEA when the sample was annealed at 873 K. Further, the same sample has produced high UTS of 996 MPa. The advantages of the VIM process are accurately controlling the speed of heating and cooling compared to the AM process and as well as the achievement of homogeneity. Moreover, the vacuum atmosphere prevents oxidation. Though, the main limitation of this technique is poor in the surface finish which needs to do secondary machining process further [75].

3.3 Directional Solidification Process

Directional solidification (DS) is a process in which the casting starts to solidify in a constrained direction and narrow/restricted passage due to which columnar grains, single grain boundaries, and improved homogeneous microstructures can be achieved. For manufacturing of HEAs through DS, the HEAs are placed inside alumina (Al_2O_3) and starts to melt due to heating system surrounding it. After solid material transfer to the liquid state, the solidification starts at the farthest point of alumina tube as shown in Fig. 23 and grows in directional as the tube pulls down into liquid coolant. Zheng et al. [76] fabricated CoCrFeNi HEA through AM under Ar gas atmosphere, re-melt the ingot five times, and then the HEA was processed through the DS process. Here, first, the HEA was melted, hold it for 60 min inside an 8 mm diameter with a length of 150 mm Al_2O_3 ceramic tube, and then the velocity of melt was varied into Ga–In–Sn coolant. After solidification in a single direction, the HEA produced a stable and homogeneous columnar grain (Fig. 24). The obtained results explained that the UTS started to increases with the function of downward velocity whereas the columnar grain size started to decreases. The fabricated CoCrFeNi HEA with 50 µm/s sample produced UTS of 0.6 GPa which was 1.39 times more compared to the same HEA processed with a velocity of 5 µm/s [77].

3.4 Infiltration Process

The infiltration process is a LSP that can also be used for fabricating the HEAs. The advantage of this process is to fabricate complex shapes made of HEAs with low percentage of porosity in a short relative time. By heating the lowest melting point elemental powders tail it melt, then either pressurized the liquid matrix phase toward the green compact or applying a capillary force as shown in Fig. 25. Mileiko et al. [78] manufactured FeCoNiCrW HEA reinforced with Al_2O_3–$Al_5Y_3O_{12}$ and Al_2O_3–$Al_5Y_3O_{12}$–ZrO_2 oxides based composites processed by liquid infiltration technique. This HEA based composite yielded a strength of around 300 MPa and retained the strength even at 1200 °C which indicated high creep strength.

3.5 Electromagnetic Stirring

Electromagnetic stirring (EMS) of liquid state method can also be used in industrial production due to its stirring efficiency which improves the quality of the product by reducing the defects and porous in the cast products. The EMS mechanism is created by collaborations of magnetic field coil (electromagnetic stirrer) and conducting metals as shown in Fig. 26a. He et al. [79] have synthesized

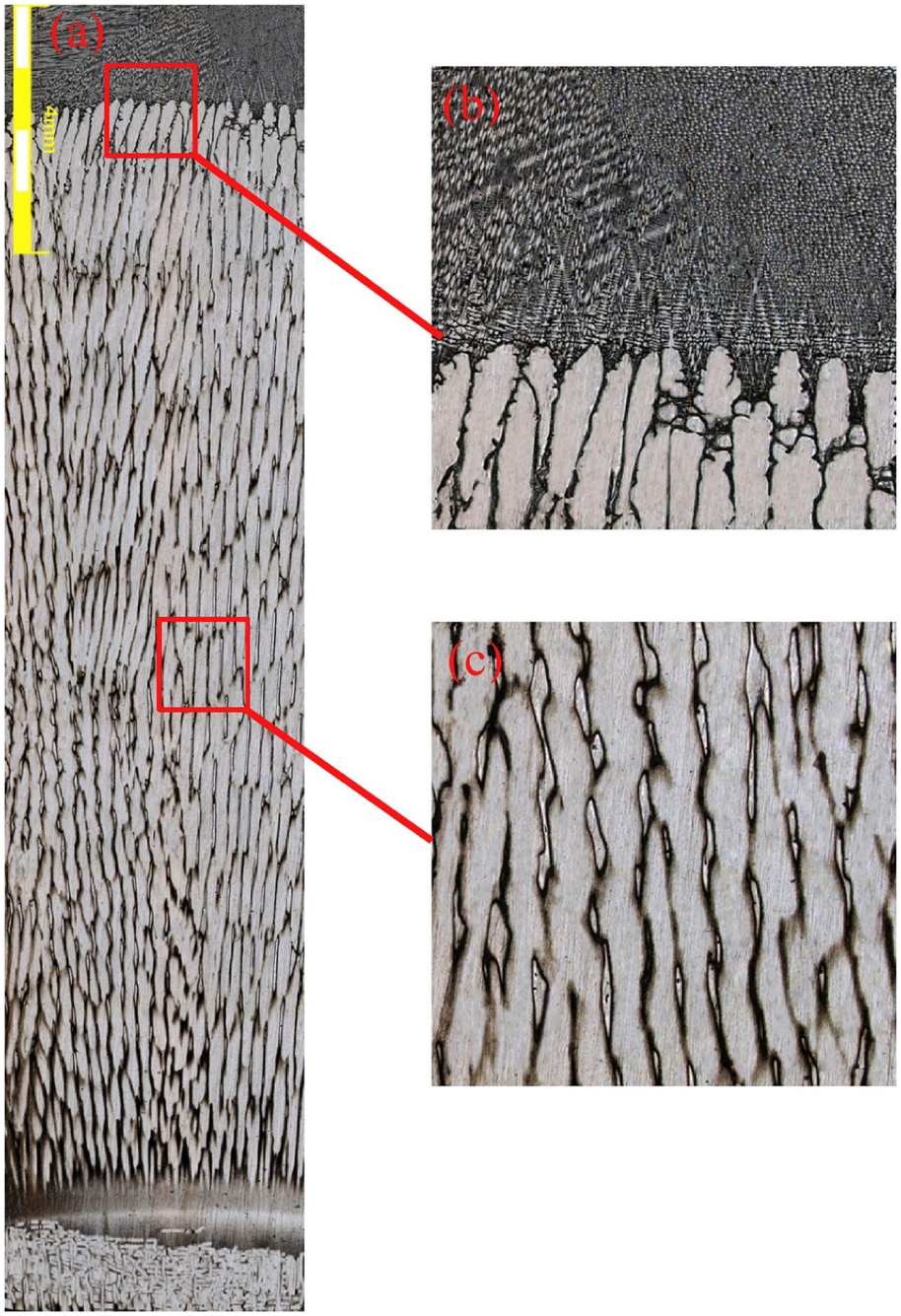

Fig. 24 Microstructure of CoCrFeNi HEA directional solidification: **a** longitudinal cross section, **b** liquid region, **c** stable solidified region [76]

a novel eutectic CoCrFeNiNbx (x = 0.1, 0.25, 0.5 and 0.8) HEAs using arc melting along with EMS. The cast alloys were re-melted with EMS five times to attain a homogeneous microstructure. For instance, the microstructure of $CoCrFeNiNb_{0.25}$ and $CoCrFeNiNb_{0.8}$ eutectic HEAs are shown in Fig. 26b, c respectively. The cast alloys have exhibited a soft FCC phase (A-region), a hard Laves phase and fine lamellar structures (spacing around 300 nm, B-region). Their main objective was to achieve a homogeneous eutectic lamellar microstructure and to have more strength with considerable ductility. The same author's group (Yuan et al. [80]) have investigated the mechanical properties of eutectic HEAs in which the hardness of 5.42 GPa, 5.87 GPa and 6.43 GPa were obtained for $CoCrFeNiNb_{0.5}$ $CoCrFeNiNb_{0.65}$ and $CoCrFeNiNb_{0.8}$ respectively. The increasing in hardness was reported due to the incorporation of Nb. Further, improved hardness and considerable ductility were obtained in $CoCrFeNiNb_{0.25}$ HEA (compressive ultimate strength of 2.025 GPa with a strain of 38.8%).

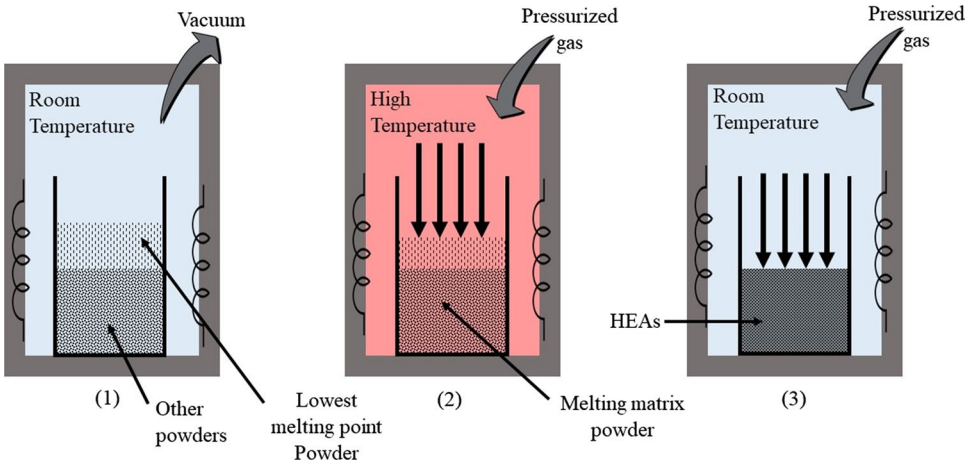

Fig. 25 Schematic diagram of the infiltration process

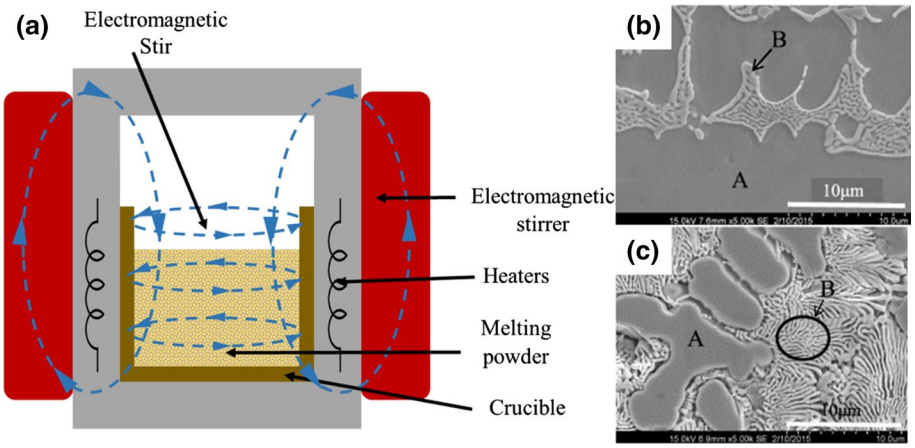

Fig. 26 **a** Electromagnetic stirring process, **b** SEM of image of cast with EMS of eutectic $CoCrFeNiNb_{0.25}$ HEA and **c** SEM of images of cast with EMS of eutectic $CoCrFeNiNb_{0.8}$ HEA [79]; A-proeuctectic FCC phase, B-Eutectic lamellar phase (Laves phase and fine laminar)

4 Thin-Film Deposition Technology

Thin-film deposition (TFD) methods (Fig. 27) can also be suggested to fabricate refractory based HEA coatings over the substrate to improve surface properties of components. A thin layer starting from 1 nm to few hundreds of microns can be deposited through advanced thin-film technology, namely, magnetron sputtering deposition (MSD), pulsed laser deposition (PLD), and plasma spraying deposition (PSD) [81]. HEAs thin-film offers improved properties in aerospace industries where high strength along with superior oxidization and corrosion resistance can be attained.

4.1 Magnetron Sputtering Process

MSD process is one of the physical vapor deposition (PVD) in which coating can be carried out under a high vacuum. This process uses mainly for producing thin films over metals, alloys, ceramics, and textiles [82, 83]. Many researchers have studied the deposition of HEA (target) by the MSD method due to its advantages as it can deposit many various materials onto the different substrate (wafer) of metals, alloys, and ceramics through the special magnetic fields. This magnetic field accelerates the deposition process and consumes low pressure compared to other techniques. Moreover, strong coating with very thin films could be achieved. Figure 28 shows the schematic of MSD where the chamber should be evacuated to at least 10^{-8} Pa; then pump the Inert gas (commonly Ar) into the chamber conferring to the desired pressure; positioning the materials which need to be coated on the anode called as the substrate (wafer) connected to DC and locating the HEA (target) on the cathode which also connected to different DC source. Due to the magnetic field which will be generated from the cathode, the Ar atoms will be ionized and impact the HEA (target) which in return release HEA particle to coat the substrate [75].

H.Kim et al. [84] developed a thin film from the single target of refractory high entropy alloy (RHEA) of NbMoTaW, in which the authors have reported a single face structure of nanocrystalline solid solution of BCC. Uniform distributions of RHEA of the substrate without any separation in large areas have been obtained. Also, TEM confirms the

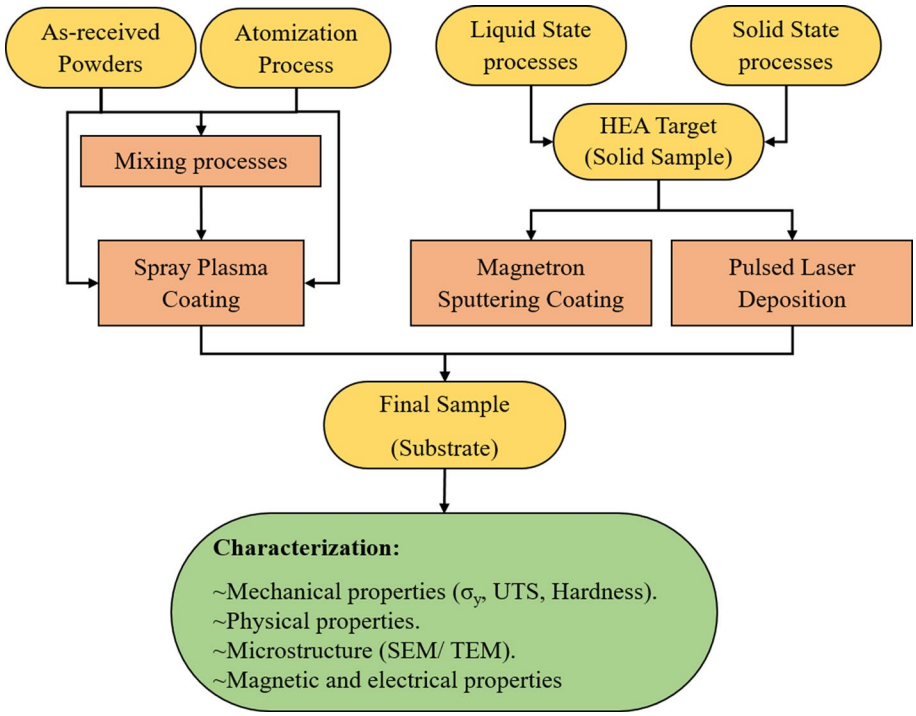

Fig. 27 Schematic showing various processing methods in thin-film depositions route for HEAs

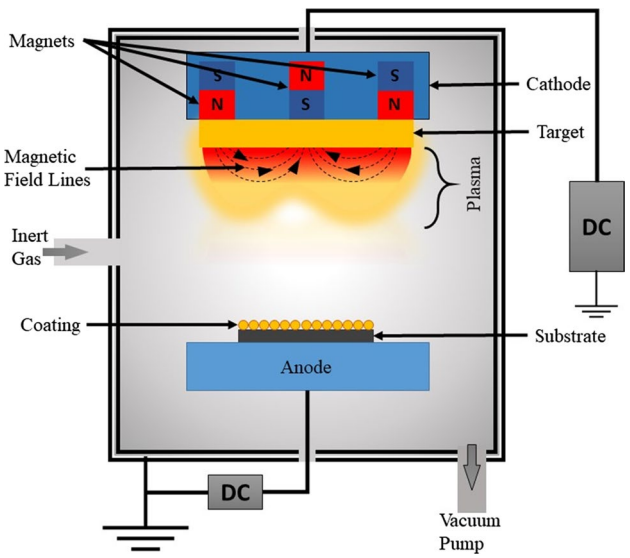

Fig. 28 A descriptive schematic of magnetron sputtering coating method

orientation of (110) BCC phase structure from the cross-section of the thin film of RHEA as a selected area. Furthermore, NbMoTaW films can act as hard protecting layers for nanofabricated devices especially for those devices that amalgamate the hardness and electrical resistivity.

4.2 Pulsed Laser Deposition

PLD is also one of the PVD technique. Several studies and many articles have published by research communities using this method due to its simple and economical process compared to other TFD methods [85]. Figure 29a shows the schematic of PLD components. An intense pulsed laser beam has concentrated on the target materials whereupon the materials are vaporized into flux of fragments material, and deposited on the substrate material as thin film under the chamber either filled with background gas [86] or high vacuum atmosphere [16, 87] to avoid any type of contaminations or interactions. On the other hand, PLD considers fast thin film technique (10–15 min) with high quality compared to other methods. Also, it is a low-temperature process due to which it can be applied to sensitive materials. However, the uneven concentration of target material on the substrate occurs and hence it may not be suitable for large scale film growth. M. Cropper [16] prepared a thin film of AlCrFeCoNiCu on borosilicate glass by PLD. Results showed that large crystal sizes of both FCC and BCC phase structures were obtained at room temperature. T.Lu et al. [87] studied the mechanical properties of the $CoCrFeNiAl_{0.3}$ HEA thin films (HEATFs) on a silicon substrate at a vacuum atmosphere, room temperature and different deposition time. The nano-hardness and young's modulus of $CoCrFeNiAl_{0.3}$ HEATFs reach 7.66 GPa and 150.35 GPa respectively. In addition, the corrosion resistance of the HEATFs was better than 316 L stainless steel. Figure 29b illustrates a clear pitting dent happened in some weak coated surface spots

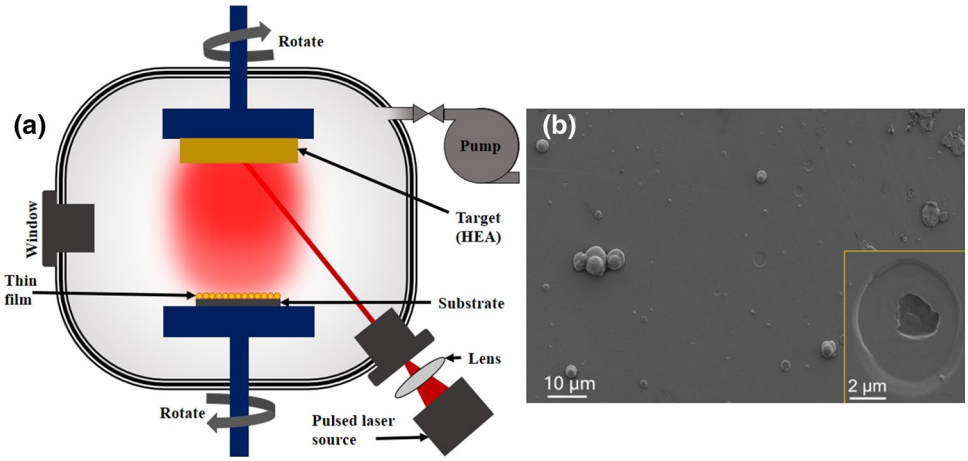

Fig. 29 **a** A descriptive schematic of pulsed lased deposition method, **b** SEM image of the HEATF after corrosion tests [87]

because of erosion, Consequently, It has been proven that thin film of HEAs can improve the mechanical and surface properties of the materials.

4.3 Plasma Spray Deposition

PSD is a process of spraying molten or semi-molten of material powders (HEA) onto substrates (wafer) for coating applications. The powders eject into elevated temperature plasma flame whereas it simultaneously heated and accelerated as shown in Fig. 30. The molten powders particles impinge the substrate surface and cool down where the coating occurs. K.Cheng et al. [88] are coated a stainless steel (304) plate (substrate) with AlCoCrFeNi HEA by the PSD process. Two groups of AlCoCrFeNi powders have prepared by the gas atomization process with a diameter of 10–60 and 60–90 µm. Then, plasma gas was set at a constant voltage of 70.5 V, and H_2 (35 l/min) gas with changing the current (500, 550, 600 650, and 750 A) and Ar flow rate (35, and 50 l/min) on one hand. It was observed that when the current and Ar flow rate was low, the spray coating of coarse powder particles has produced the un-melted regions over the substrate as shown in Fig. 31a. However, effective coating and properly melted regions were obtained for the spray coating of fine powder particles at the same lower voltage and flow rate. But this sample exhibited some solid powder particles drop (Fig. 31b). On the other hand, when the current and Ar flow rate were set at higher values, both the coated powder particles over the surface exhibited a perfect, flat, and flaw-free coating (Fig. 31c). Besides, the observed hardness value was proportionally increased with the increase of current and an Ar flow rate; the noticed highest hardness value of fine particles and coarse particles was 249 and 427 HV respectively.

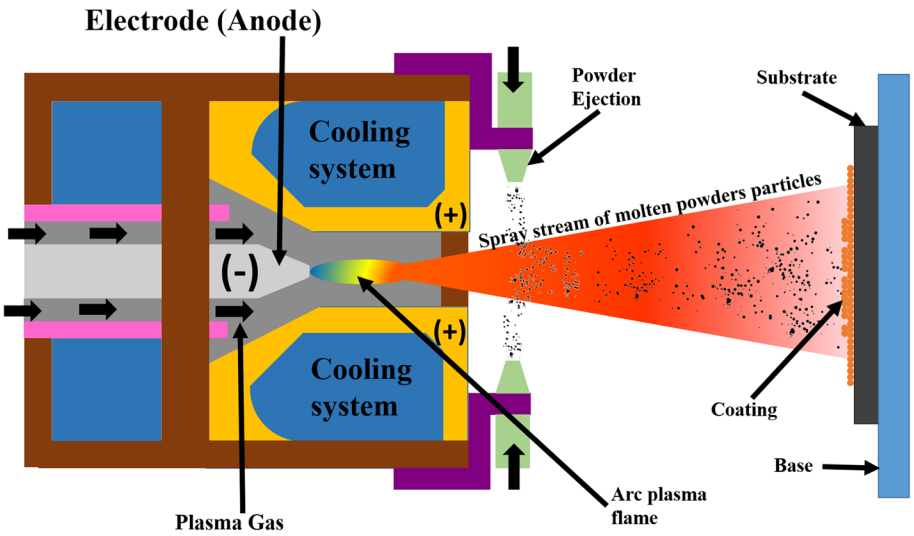

Fig. 30 Schematic of the plasma spray coating process

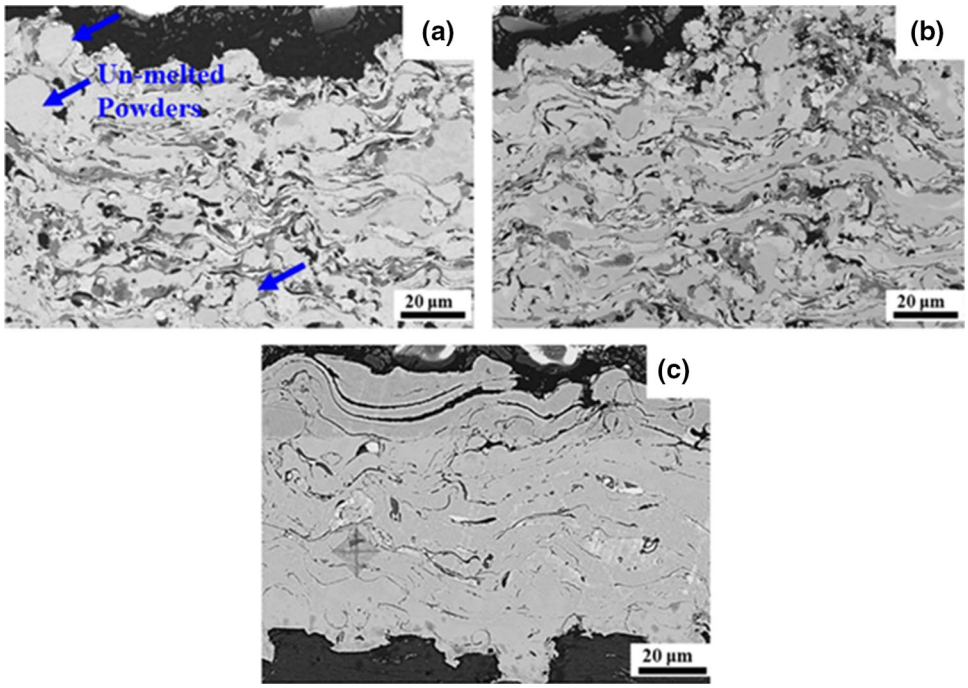

Fig. 31 Cross-sectional SEM images of **a** i-500-35, **b** i-600-50, and **c** ii-750-50 samples [88]

5 Additive Manufacturing Technology (AMT)

HEAs are being manufactured using the above-mentioned SSP (Sect. 2) and LSP route (Sect. 3) in which AM and or SPS are the commonly used techniques. However, it is very difficult to produce HEAs with homogeneous structure by AM, refined grain structure and maintaining single phase SS using MA followed by SPS. Further, the manufacturing of HEAs in the industrial scale is also not feasible using conventional methods. Nevertheless, there is potential demand in HEAs for specialized applications that need to fabricate the HEAs with less complex technique, high level of controlling the process to have specified internal structure and to fabricate quickly. Further, based on current research, these are possible by laser-based AMT [89]. In AMT, the parts are being fabricated layer-by-layer which has different techniques, namely, fusion deposition modeling, stereolithography, 3D plotting, selective laser sintering (SLS), selective laser melting (SLM), selective electron beam melting (SEBM), and laminated object manufacturing. Among these techniques, laser-based SLS/SLM can be used to manufacture the products from HEAs which has several features: produce parts at high temperature in a short duration, faster cooling rate, specific microstructure, avoiding of unwanted phases, flexible and designing the parts in a rapid manner, produce highly intricate parts economically, lesser skill force for manufacturing, effective material utilization (net shape), and ability to change the part design using software [90, 91]. Figure 32 shows the schematic of the working principle of SLM in which a high power laser beam (~ 200 to 1000 W) is used to melt the selective places over the powders to print one layer. The fiber laser with a wavelength of around 1000 nm can be used for printing. This laser is controlled by Galvanometer, lens and then directed over the target surface. The powder materials start to melt using the laser power consequently the melted powders start to solidify. This SLM consists of two platforms, namely, powder delivery platform and powder build platform. The table in the powder build platform can move along z-direction whereas the laser scanning system can move along x–y directions. After printing one layer, the activated roller transfers the required

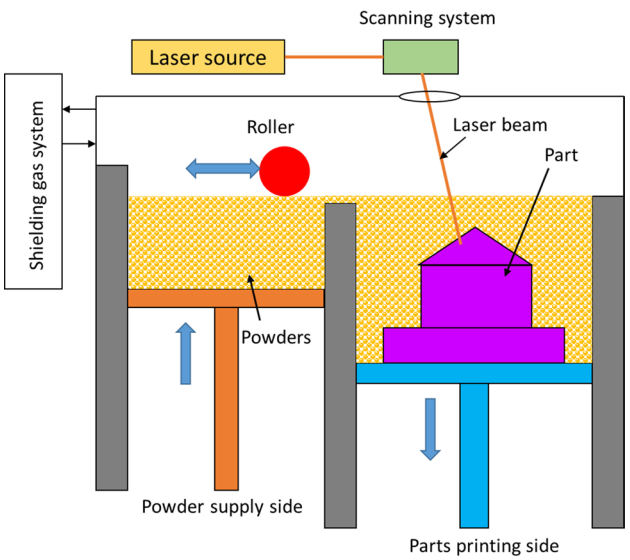

Fig. 32 Schematic of working of selecting laser melting (SLM)

amount of powders from the powder delivery side to the build side. Again, another layer can be printed using a laser system. This is the step that repeats continuously until the entire object is built. The entire SLM system is controlled by shielding gas to avoid oxidization. Several process parameters influence the product quality which is laser power, scanning speed, focal laser beam diameter, laser scanning path, and layer thickness.

The raw powders for SLM should be in the form of a sphere to have improved performances for which gas atomization is being used to synthesize the HEAs powders [34, 35]. Li et al. [91] investigated CoCrFeMnNi HEA processed by SLM. These HEA powders were synthesized by gas atomization in which the average particle size was 36 µm with a spherical shape. After synthesizing the powders, the HEA powders was printed using SLM in which the used laser power (P) was 400 W, laser beam diameter was 90 µm, and layer thickness (t) was 0.03, and the authors varied the scanning speed (v) from 800 to 4000 mm/s. Due to varying the scanning speed, the volumetric energy density (VED) was varied which can be determined using eq. (1):

$$VED = \frac{P}{vht} \tag{1}$$

After printing the sample, HIPing was used to increase the density of the sample. The results were explained that the printed sample density was started to increases steadily with the function of VED and then decreases at high value of VED. From XRD results, the observed full width half maximum (FWHM) at the major peak was started to broaden with the function of VED and the corresponding lattice parameter also changed. The microstructures of the SLM printed sample exhibits a large number of dislocations and more lattice distortion. The printed sample produced a tensile strength of 600 MPa whereas the HIPed sample exhibited 650 MPa. This result indicates obviously that HEAs with specified internal microstructure can be easily manufactured using recent AMTs. Joseph et al. [92] manufactured $Al_xCoCrFeNi$ HEAs (x = 0.3, 0.6, 0.85) through direct laser fabrication (DLF), DLF/HIPing, and arc melting (5 re-melts). Very fine elongated grains were obtained in the DLF method, somewhat coarse grains were obtained in DLF/HIPing method, and very big dendrites microstructures were obtained in the AM method (Fig. 33a–c). Further, mechanical properties results explained that $Al_{0.6}CoCrFeNi$ HEA consolidated by DLF/HIPing method exhibited improved mechanical properties in terms of compressive strength and ductility when compared to other methods. This sample produced around 1.6 GPa compressive strength with a true strain of 0.75. This was due to the presence of coarse BCC and B2 phases which enhanced the ductility with considerable strength.

6 Microstructural Changes, Mechanical Properties Variations, and Major Challenges of HEA

Phase stability is the important feature in HEAs which can be achieved by high configurational entropy that depends on number the of elements, atomic ratios, and structural parameters of each element. The presence of high configurational entropy decreases the amount of free energy in HEAs according to Gibbs free energy equation (see "Appendix of ESM") due to which stabilized solid solutions phase can be obtained even at high temperatures. Among the discussed manufacturing methods, gas atomized HEAs powders (Fig. 4) followed additive manufacturing technology (Fig. 32), MA powders (Fig. 7 followed SPS (Fig. 14), vacuum induction melting (Fig. 22), directional solidification (Fig. 23), magnetron sputtering (Fig. 28), and laser deposition (Fig. 29) techniques can produce single phase-stable HEAs by which extensive mechanical properties could be obtained. This meant, the formation of second phase particles/precipitates, and or IMCs can almost be stopped due to less processing time for which the HEAs will not have a time for unwanted reactions that develops the second phase/IMCs. Most of the HEAs produces a single phase with FCC, and, or BCC crystal structures. Some HEAs produces HCP crystal structure. Superior mechanical properties of HEAs can be obtained based on the type of crystal structure formation, the number of phases (single phase, two-phase, multiphase) and processing routes.

However, mostly, the phase formation of HEAs is in multiphase (Two or more) which also helps to enhance the properties according to the need. For example, simultaneous improvement in mechanical strength and ductility can be achieved by dual-phase in HEAs. The presence of the soft phase in HEAs increases the ductility whereas the hard phase increases the yield strength. Similarly, the presence of multi-phases in HEAs can increase the mechanical properties, namely, YS, ductility, elastic modulus, plastic modulus, UTS, fatigue, creep etc… Synthesizing a single-phase SS of HEAs (usually supersaturated and sometime metastable phase) by SSP route can undergo various phase transformations during heat treatment and sintering which leads to forming two-phase transformation, namely, eutectoid and precipitation. Due to these phase transformations, all the atoms are to be rearranged to form a new phase(s). The newly transformed phases maybe two or more which may be eutectoid, sigma/laves phase, precipitates, and spinoidal decomposition.

Moreover, the heat treatment of HEAs influences mechanical properties considerably. For instance, AlCoCrFeNi HEA in as-cast and heat-treated behavior is illustrated that an improvement in ductility with plastic strains as the aged

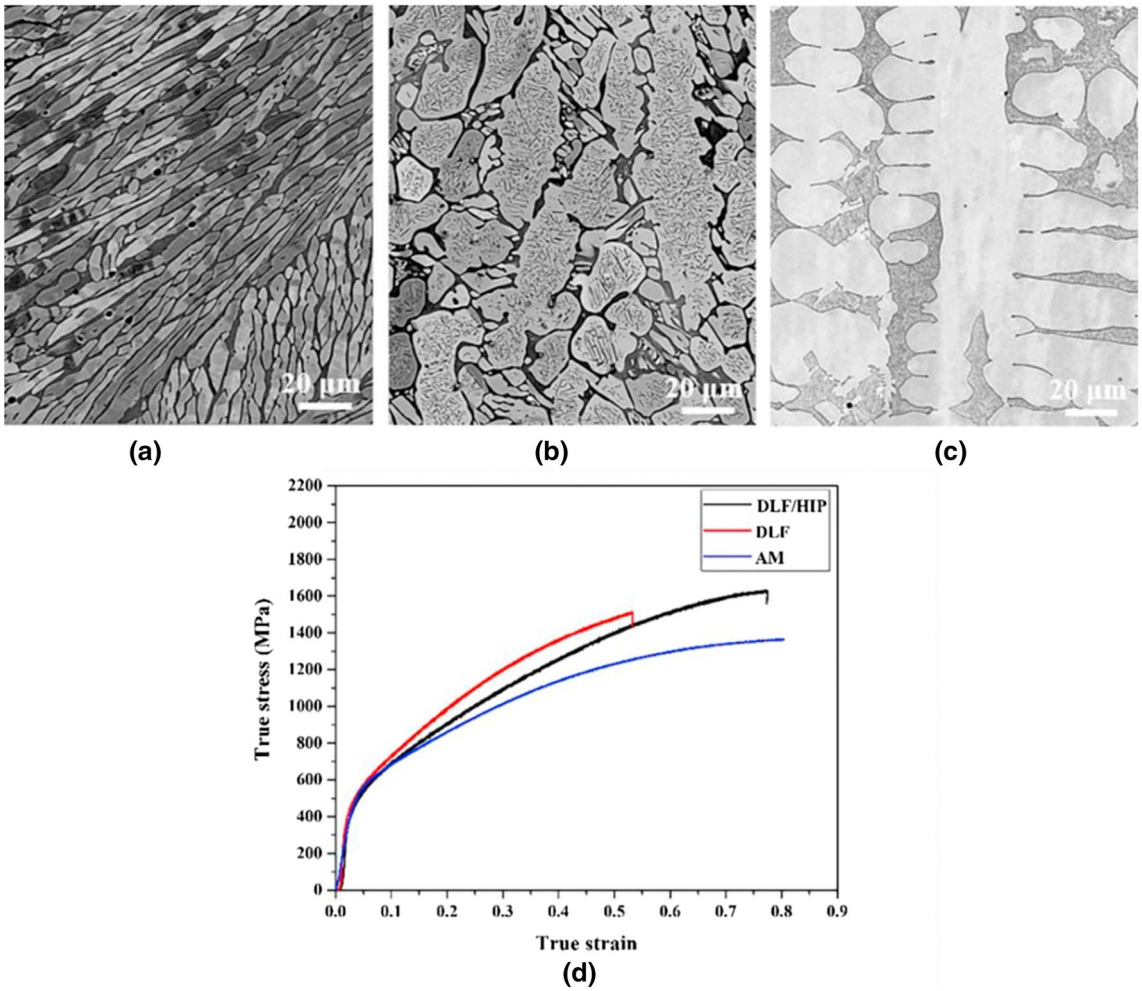

Fig. 33 **a**–**c** SEM images of $Al_{0.6}CoCrFeNi$ HEA prepared by different route: **a** direct laser fabrication (DLF), **b** DLF followed by HIPing, **c** arc melting; **d** true stress-true strain curves of $Al_{0.6}CoCrFeNi$ HEA at different manufacturing methods (Joseph et al. [92])

temperature increases [93]. Rao et al. [94] investigated the aging behavior of $Fe_{0.4}Cr_{0.4}NiMnCu$ HEA which was aged at two different temperatures (900 °C and 1000 °C for 24 h (Fig. 34). From Fig. 34a, b, it was ensured a homogenized FCC phase and a small amount of dendrite phase in the form of needle-like shapes after aging. The HEA aged at 900 °C was exhibited interdendritic phase whereas HEA aged at 1000 °C was exhibited uniform dispersion of needle-like phase which corresponds to the BCC phase. The XRD pattern of Fig. 34c for HEA aged at 1000 °C was clearly shown the formation of the BCC phase which was conformed as per Fig. 34b. The true stress-true strain curves of as-cast and homogenized $Fe_{0.4}Cr_{0.4}NiMnCu$ HEA is also shown in Fig. 34d. The result was explained that homogenized HEA exhibited more strength when compared to as-cast one. However, a homogenized HEA sample produces decreased ductility due to dendrite BCC phase precipitates. Therefore, it is clear that the properties of HEAs are highly influenced by the phase formation, various processing methods, and types of elements present in HEAs. This section correlates the propertie's improvement in terms of phase formations, microstructural variations, and stress–strain curves.

In line with previous studies, all HEAs produces extensive mechanical properties with considerable elongation to failure even at a high temperature which is an important property needed for high-temperature applications. Based on the literature, it was observed that the HEAs manufactured from LSP route, the amount of SS strengthening of elements, and the amount of precipitates strengthening are the two main mechanisms that promotes the mechanical properties of HEAs. However, in the SSP route, especially for MA, and AMT, grain boundary strengthening, dislocation strengthening and strengthening by precipitates are the major mechanisms that involves mechanical properties improvement. Figure 35 shows the tensile strength with the function of elongation-to-failure for conventional materials and some HEAs [56]. From Fig. 35, it is very clear that HEAs exhibits considerable strength with improved ductility. For instance,

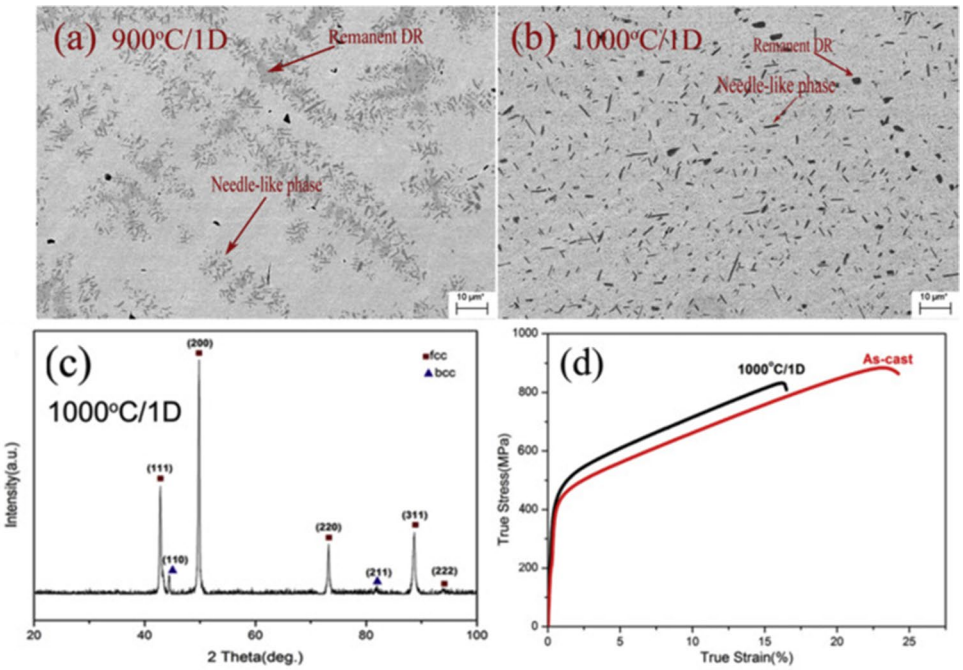

Fig. 34 **a** and **b** Backscattered electron SEM images of homogenized $Fe_{0.4}Cr_{0.4}NiMnCu$ HEA at two different temperatures after 24 h, **c** corresponding XRD pattern of 1000 °C homogenized sample, and **d** true stress-true strain curves of as-cast and homogenized at 1000 °C HEAs. [94]

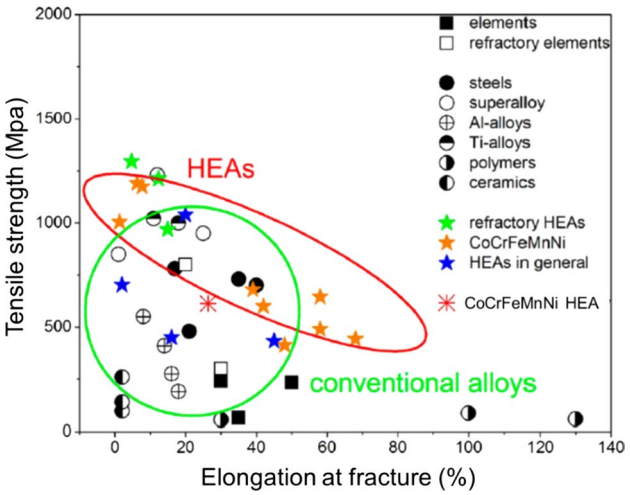

Fig. 35 Comparison of tensile strength between conventional materials and some HEAs [56]

the REHEAs produces the tensile strength of 3 times higher than steels and 5 times more than Al-alloys.

The implications of Mechanical properties are shown in Table 3 which illustrates the summary of the manufacturing method of some HEAs, main objectives of each work, and the outcome of mechanical properties. Table 3 was explained that the majority of the researchers tend to use the AM process because of fast productivity where there is no need to do secondary operations to produce the final sample such as the compaction process for producing a green sample or sintering processes to increase the bonding in case of PM route. In contrast, it was found that the MS technique was rarely used in the fabrication of HEAs [95–101]. Besides, the majority of research studies have concentrated on the microstructure of the alloy and the mechanical properties through either tensile and compressive tests or hardness tests. For instant, VHS values ranges from 0.141 to 5.8 GPa was achieved in $CoCrFeNiTa_{0.4}$ HEA [102]. Further, some studies have investigated the corrosion behavior of HEAs [70, 71, 93, 103]. It was also observed from Table 3 that the tensile strength and hardness were decreased slightly as the temperature started to increase in all the HEAs. The mechanical behavior of some HEAs is shown Fig. 34. The variation of the atomic fraction of some element(s) in HEAs influences much on mechanical behavior. For instance, The UTS of $CoCrFeNiTa_{0.4}$ HEA exhibited more value compared to $CoCrFeNiTa_{0.75}$ HEA [102] likewise, $Al_{0.3}CoCrFeNiMn_{0.3}$ has UST of 371MPA more than $Al_{0.3}CoCrFeNiMn_{0.1}$ which has exhibited UST of 336 MPa [99]. The refractory high entropy alloys (RHEAs) also reduce a slight increase in strength and hardness as the Ti and C volume fraction increased in $Ti_xNbMoTaW$ and $Mo_{0.5}NbHf_{0.5}ZrTiC_x$ HEAs respectively [104, 105]. Also, the compression ductility of HEAs started to increases while the strengths and elastic modulus diminishes [25, 106–108] at elevated temperature. For instance, the compressive strain of around 27% was obtained in TiNbMoTaW REHEA whereas TiVNbTaMoW HEA produced the compressive strain of only 4% [106]. Some other research articles demonstrate the mechanical properties change by varying any one element in HEA. Incorporation of Ti_x in $Ti_xNbMoTaW$ HEA increases the UTS with an increment

Table 3 Summary of literature results illustrating manufacturing methods of HEAs, objective(s) each researcher work, and mechanical properties results

Composition	Methods of preparing HEA	GAP(paper's goals)	Hardness (HV)		Strength (MPa)	References
$CoCrFeNiTa_X$	Arc melting in an Ar atmosphere re-melted five times	Influence of Ta addition microstructures and mechanical properties of $CoCrFeNiTa_X$ HEAs	X	HV	σ_y	[102]
			0	141	145	
			0.1	180	267	
			0.2	277	405	
			0.3	365	946	
			0.4	492	1316	
			0.5	498	1346	
			0.75	550	–	
$AlMo_{0.5}NbTa_{0.5}TiZr$	Vacuum arc melting (re-melted five times)	Investigate the microstructure, phase evolutions and mechanical properties of $AlMo_{0.5}NbTa_{0.5}TiZr$ and $Al_{0.4}Hf_{0.6}NbTaTiZr$ HEAs at elevated temperature	T (C°)	HV	σ_y	[107]
			20	592	2368	
			800		1810	
			1000		772	
			1200		275	
$Al_{0.4}Hf_{0.6}NbTaTiZr$			T (°C)	HV	σ_y	
			20	500	2269	
			800		834	
			1000		455	
			1200		135	
TaNbHfZrTi	Vacuum arc-melting then hot isostatic pressing (HIP) (re-melted three times)	Synthesize, characterize, and mechanical behavior of $Ta_{20}Nb_{20}Hf_{20}Zr_{20}Ti_{20}$ HEA at room temperature	HV	σ_y		[111]
			391	929		
$Al_{0.3}CrFe_{1.5}MnNi_{0.5}$	Arc-melting process, re-melted five times Then casting.	Synthesize $Al_{0.3}CrFe_{1.5}MnNi_{0.5}$ HEA by arc melting, investigate the aging behavior on microstructures and its mechanical properties.	T_{Age} (°C)	HV		[66]
			As- cast	298.8		
			650	636.2		
			750	898.5		
$Al_xCoCrFeNiTi_{1-x}$ (x = 1.0, 0.8, 0.5)	~arc-melting process re-melted at least five times. then casting under vacuum	Investigate the role of Al and Ti in $Al_xCoCrFeNiTi_{1-x}$ HEAs on microstructures, mechanical behavior and corrosion resistance.	x	HV		[112]
			1	542.9		
			0.8	472.6		
			0.5	520.4		

Table 3 (continued)

Composition	Methods of preparing HEA	GAP(paper's goals)	Hardness (HV)		Strength (MPa)	References
$CoFeNiMnTi_xAl_{1-x}$	Arc-melting process	Investigate the deformation behavior of $CoFeNiMnTi_xAl_{1-x}$ HEAs, study the corresponding microstructures and mechanical properties.	X	HV	σ_y	[113]
			0	455.2	577.4	
			0.1	525.5	926.7	
			0.3	250.1	1106.6	
			0.5	518.7	1052.8	
			0.8	530.6	1125.8	
			1	708.4	1070.5	
$(Al_7Co_{24}Cr_{21}Fe_{24}Ni_{24})_{100-x}Cr_x$	Vacuum-arc-melting method remelted 6 times	Examine the influence of Cr content in $(Al_7Co_{24}Cr_{21}Fe_{24}Ni_{24})_{100-x}Cr_x$ HEAs on its microstructures and mechanical properties.	X	HV	σy	[114]
			0	150 ± 5	249 ± 6	
			11	300 ± 3	456 ± 9	
			20	420 ± 4	998 ± 7	
			26	510 ± 5	1649 ± 4	
$Al_xHfNbTiZr$ (x = 0–1.5)	Arc melting in an Ar atmosphere re-melted five times	Investigate the effect if Al addition in $Al_xHfNbTiZr$ HEA on microstructures and mechanical properties changes.	X	HV	σ_y	[115]
			0	242 ± 8	706	
			0.5	338 ± 6	1120	
			0.75	412 ± 8	1331	
			1.0	452 ± 11	1582	
			1.25	496 ± 9	1620	
			1.5	527 ± 8	1746	
MoNbHfZrTi (as- cast) MoNbHfZrTi (as-homogenized)	Vacuum arc-melting (re-melted five times)	Investigate the microstructure and mechanical properties of MoNbHfZrTi under as-cast and as-cast with homogenized conditions at different temperatures.	T (°C)	HV	σ_y (UTS)	[116]
			25		1719 (1803)	
			25		1575 (1640)	
			800		825 (1095)	
			900		728 (938)	
			1000		635 (654)	
			1100		397 (399)	
			1200		187 (194)	
CoCrFeNi	Arc-melting under an argon atmosphere, re-melted at five times. Directional solidification process.	Fabricate HEA with DS process with different flow velocity (X = 5, 10, 20, and 50 μm/s)and study microstructure and mechanical behavior of HEA with high strength and superior ductility. With	X	HV	σ_y, (UTS)	[76]
			5		233,(383)	
			10			
			20			
			50		390,(596)	

Table 3 (continued)

Composition	Methods of preparing HEA	GAP(paper's goals)	Hardness (HV)		Strength (MPa)	References
CoCrFeNiCu	Arc-melting under an argon atmosphere, re-melted at five times. Directional solidification process.	Investigate the microstructure evolution and tensile properties of HEA synthesized by DS with growth rate (X = 10, 30, 60, and μm/s). study the relationship between the microstructure and solidification parameters.	X	HV	UTS	[77]
			10		400	
			30			
			60			
			100		450	
$Mo_{0.5}NbHf_{0.5}ZrTiC_x$	Arc melting argon atmosphere(re-melting for five time	Investigate the mechanical properties and deformation behavior of $Mo_{0.5}NbHf_{0.5}ZrTiC_x$ HEAs	X=	HV	σ_y (UTS)	[105]
			0		~1192 (1500)	
			0.1		1183 (2139)	
			0.3		1201 (1965)	
HfMoNbTaTiZr	Vacuum arc melting)re-melted five times(	Investigate the mechanical properties of HfMoNbTaTiZr and HfMoTaTiZr HEAs at different temperatures.	Tem	HV	σ_y	[25]
			25 °C		1512	
			800		1007	
			1000		814	
			1200		556	
HfMoTaTiZr			Tem	HV	σ_y	
			25 °C		1600	
			800		1045	
			1000		855	
			1200		404	
TiNbMoTaW	Vacuum arc melting)re-melted five times(	Investigate the effect of Ti incorporation in TiNbMoTaW, and TiVNbMoTaW HEAs on mechanical behavior at different temperature.	Tem	HV	UTS	[106]
			25		2005	
			600		1681	
			800		1618	
			1000		1426	
			1200		814	
TiVNbMoTaW			25 °C	HV	UTS	
			600		2135	
			800		1590	
			1000		1180	
			1200		1105	

Table 3 (continued)

Composition	Methods of preparing HEA	GAP(paper's goals)	Hardness (HV)		Strength (MPa)	References
$Ti_xNbMoTaW$	Vacuum arc melting (re-melted five times)	Examine the mechanical behavior of refractory based $Ti_xNbMoTaW$ HEAs	X=	HV	UTS	[104]
			0		1148	
			0.25		1197	
			0.5		1500	
			0.75		1593	
			0.1		1910	
CoCrFeNi (as-cast)	Vacuum Arc-melting. re-melted at least five times Solidified by supercooling method	Investigate the microstructures and mechanical properties of CoCrFeNi HEA under as-cast and undercooling conditions.		HV	σy	
					137	[23]
CoCrFeNi (undercooling)					455	
$Fe_{43.45}$-$Ni_{27.5}$-$Co_{17.5}$-$Al_{11.5}$-$B_{0.05}$	Arc-melting. (re-melted eight times) Hot rolling process	Investigate and optimize the heat treatment parameters (annealing temperature, time, annealing condition) on FeNiCoAlB, FeNiCoAlTaB, FeNiCoAlCrB HEAs				[117]
$Fe_{40.95}$-$Ni_{27.5}$-$Co_{17.5}$-$Al_{11.5}$-$Ta_{2.5}$-$B_{0.05}$	Arc-melting Hot rolling process					
$Fe_{34.95}$-$Ni_{27.5}$-$Co_{17.5}$-$Al_{11.5}$-$Cr_{8.5}$-$B_{0.05}$	Arc-melting Cold rolling process Annealing process ~ CG-1200 ~ CG-1300				~175	
					~150	
$AlCr_xNbTiV$ (x = 0 - 1.5)	Arc-melting process	Study the influence of heat treatment (annealing, 800 °C, 1000 °C for 100 h) of $AlCr_xNbTiV$ HEA on microstructure and mechanical properties.	X	HV	σy	[118]
			0		1000	
			0.5		1300	
			1.0		1550	
			1.5			
$AlNbTiVZr_x$			X	HV	σy (MPa)	
			0		1000	
			0.5		1485	
			1.0		1500	
			1.5		–	
$Al_{0.5}CoCrFeNi$	Vacuum arc melting re-melted four times	Influence of heat treatment on microstructure and mechanical behavior of Al0.5CoCrFeNi HEA		594		[119]
$HfMo_{0.5}NbTiV_{0.5}Si_x$	Induction levitation melting argon atmosphere (re-melt two times)	Investigate the mechanical behavior of $HfMo_{0.5}NbTiV_{0.5}Si_x$ HEAs	X=	HV	σ_y (UTS)	[72]
			0	403	1260 (—)	
			0.3	500	1617 (2016)	
			0.5	570	1787 (2052)	
			0.7	612	2134 (2242)	
$Al_{25}Ti_{25}Ga_{25}Be_{25}$	Induction-melting furnace under Ar atmosphere.	Investigate mechanical behavior and the corrosion behavior of $Al_{25}Ti_{25}Ga_{25}Be_{25}$ HEA using electrochemical polarization method		HV	UTS	[120]
			As-cast	490 ± 10	1620	
			Annealed	490 ± 20		

Table 3 (continued)

Composition	Methods of preparing HEA	GAP(paper's goals)	Hardness (HV)		Strength (MPa)	References
$Al_{0.3}CoCrFeNiMn_x$	Induction melting and casting in air	Examine the influence of Mn incorporation in $Al_{0.3}CoCrFeNiMn_x$ HEAs on microstructures, mechanical and electrochemical corrosion behavior	x	HV	σ_y (UTS)	[99]
			0	141	119 (295)	
			0.1	~146	149 (336)	
			0.3	156	158 (371)	
$Al_{0.5}CoCrCuFeNi$	Powders melted by the medium frequency induction melting furnace (electromagnetic stirring (EMS))under low vacuum condition	Examine the grain refinement by electromagnetic stirring, microstructure and mechanical properties changes in $Al_{0.5}CoCrCuFeNi$ HEA.		HV	UTS	[69]
			With EMS		693.66	
			Without EMS		616.76	
$Al_{0.3}CoCrFeNi$	Induction melting from powders of pure metals. Re-melted 3 times	Investigate phase changes, structural evolution and hardness changes in $Al_{0.3}CoCrFeNi$ HEA at high temperature, high temperature along with high pressure		——		[15]
$Al_2CoCrFeNi$				568		
$Al_2CoCrFeNi$ +3 at% Sc.				622		
$Fe_{20}Co_{20}Ni_{20}Cr_{20}Mn_{20}$ (Ho)	Ball milled under Ar gas then Powder sintering	Study of microstructure and mechanical behavior of FeCoNiCrMn HEA by varying Al content and process parameters (MA, time, sintering temperature)	T_{sinter} °C	HV	UTS	[28]
			1200	1200	328	
			1300	1500	410	
			1400	3200	875	
$Fe_{20}Co_{20}Ni_{20}Cr_{20}Mn_{20}NaCl_{0.1}$ (HoNa)			1200	1700	465	
			1300	2000	547	
			1400	2500	683	
$Fe_{18.8}Co_{18.8}Ni_{18.8}Cr_{18.8}Mn_{18.8}Al_6$ (H_3Na)			1200	1700	465	
			1300	1500	410	
			1400	3400	929	
$Fe_{18}Co_{18}Ni_{18}Cr_{18}Mn_{18}Al_{10}$ (H_5Na)			1200	1300	328	
			1300	1200	410	
			1400	3700	875	
FeCoCrNiMnTi0.1C0.1	Mechanical alloying (MA) Vacuum hot-pressing sintering (VHPS)	Study the microstructure and the mechanical behavior of FeCoCrNiMnTi0.1C0.1 at different temperature of VHPS (850, 900, 950 and 1000 °C)	T_{sinter} °C	HV	σ_y (UTS)	[121]
			850	457 ± 2	1616 (1868)	
			900	461 ± 3	1652 (1983)	
			950	428 ± 3	1490 (1962)	
			1000	378 ± 4	1194 (2008)	

Table 3 (continued)

Composition	Methods of preparing HEA	GAP(paper's goals)	Hardness (HV)		Strength (MPa)	References
$FeCoCrNiMnAl_x$	Mechanical alloying (MA) Vacuum hot-pressing sintering (VHPS) at 900 °C and 50 MPa	The effect of Al concentration of (0, 0.1, 0.3, 0.5, 0.7, and 1.0) on $FeCoCrNiMnAl_x$ HEA to improve the hardness and strength	X	HV	σy (UTS)	[42]
			0	415	1314 (2026)	
			0.1	432	1631 (2086)	
			0.3	511	1836 (2341)	
			0.5	553	1932 (2376)	
			0.7	622	2230 (2552)	
			1.0	684	– (2406)	
$AlFeCuCrMg_x$	Mechanical alloying (MA) Vacuum Spark Plasma Sintering (SPS) 700 °C and 50 MPa	Investigate the microstructure, phase evolution and transformation. Mechanical properties have been investgated.	X	HV	σy	[122]
			0	650	1950	
			0.5	853	2559	
			1.0	750	2220	
			1.7	533	1559	
$Al_2CoCrCuFeNiTi_x$ (x = 0.0, 0.5, 1.0, 1.5)	Ball milling for 24 h then Laser cladding.	Investigate the laser coating of $Al_2CoCrCuFeNiTi_x$ HEA on Q235 steel substrate on microstructure, hardness and corrosion properties.	x	HV		[123]
			0	780		
			0.5	960		
			1.0	850		
			1.5	988		
$Al_{0.5}FeCu_{0.7}NiCoCr$	Ball mill for 2 h (mixing) then laser cladding method	Investigate the effect of structural and mechanical properties changes after laser cladding of $Al_{0.5}FeCu_{0.7}NiCoCr$ HEA on the Al substrate	HV			[95]
			750			
FeCoCrNi (Arc melter)	Gas Atomization Process then Selective Laser Melting And arc melting process	Synthesize FeCoCrNi HEA through selective laser melting, investigate the mechanical properties and then compared the results with arc melted sample	188	118		[113]
FeCoCrNi (AM 50 µm)			402	205		
FeCoCrNi (AM 20 µm)			600	238		
$Al_{0.5}$ CoCrCuFeNi	Gas Atomization Process then Additive Manufacturing	Synthesizing AlCoCrCuFeNi HEA powders through gas atomization technique, then investigate the microstructures and mechanical behavior, compared with cast alloy	HV			[124]
			200.5 ± 8.7			
$Al_{0.5}$oCrCuFeNi$Si_{1.2}$			751.8 ± 13.9			
$Al_{0.5}CoCrCuFeNiSi_{2.0}$			747.4 ± 10.8			
AlCoCrFeNi	Direct laser fabrication (DLF)	Investigate the microstructure, mechanical behavior and corrosion properties of AlCoCrFeNi HEA by DLS at different aged condition.	T_{age}	HV	UTS	[93]
			600		1310	
			800		1170	
			1000		1070	
			1200		1130	

Table 3 (continued)

Composition	Methods of preparing HEA	GAP(paper's goals)	Hardness (HV)		Strength (MPa)	References
			X	HV		
$Al_XCoCrFeNi$	Gas atomization then Direct laser fabrication (DLF) And vacuum arc melting re-melted four times	Comparison and investigation of different processing method of $Al_XCoCrFeNi$ HEAs through direct laser sintering, and arc melting. The σy of both process HEAs was the same, but different in ductility.	0.3		σy 200	[92]
			0.6		~400	
			0.85		~1400	

amount of 66.4% [104]. $HfMo_{0.5}NbTiV_{0.5}Si_x$ HEA exhibited improved mechanical properties in terms of strength and hardness by the addition of silicon [72]. The tensile yield strength of $HfMo_{0.5}NbTiV_{0.5}Si_{0.7}$ exhibited 1.69 times higher value compared to $HfMo_{0.5}NbTiV_{0.5}$ HEA. Further, Guo et al. [105] manufactured a HEA based composite which consists of $Mo_{0.5}NbHf_{0.5}ZrTi$ HEA matrix reinforced with carbide particles that produced improvements in compressive strength and plasticity. $Mo_{0.5}NbHf_{0.5}ZrTiC_{0.3}$ HEA produced a compressive yield strength of 2.14 GPa with a 38.9% strain whereas $Mo_{0.5}NbHf_{0.5}ZrTi$ HEA matrix exhibited the compressive yield strength of 1.54 GPa with 24.6% strain.

Various manufacturing methods are available to manufacture different HEAs as discussed in the previous sections. The major manufacturing methods are SSP, LSP, and TFD. LSP route can be used to fabricate the HEAs in the forms of rods, billet, and bars. From these forms, products can be fabricated. Mostly, VAM and or VIM methods are suggested to fabricate the parts. For instance, among these two methods, the VAM process produces good and defect-free casting due to the high vacuum involves comparing to the VIM process. The AM $Al_{0.5}CrFeCoNiCu$ HEA produced straight homogeneous dendrites in all orientations whereas the VIM process produced non-uniform dendrites-like along with coarse grain structure for the same HEA. Besides, the AM HEA sample shows single-phase FCC-structure while the VIM sample produced dual-phase FCC and BCC structures [75]. However, evaporation of low melting elements, controlling of required composition, and formation of heterogeneous microstructures are the major drawbacks in the LSP route. To overcome these issues, the SSP route can be recommended in which the components can be manufactured directly from the HEAs powders followed by advanced consolidation methods (MA and SPS). Single-phase/homogeneous microstructures can be achieved via the SSP technique with high quality. Though it is a relatively expensive process, this technique can give improved mechanical properties. For comparison between AM and MA technique as an example, Baldenebro-Lopez et al. [49] fabricated AlCoFeMoNiTi HEA by MA with BPR of 1:5 for 10 h under argon atmosphere. The HEA powders were pressed in a die with a compaction pressure of 1.5 GPa (green samples); then sintered at 1423 K under Ar atmosphere for 3 h. In parallel, some of the same green samples were melted in the AM process under Ar atmosphere (re-melted five times to have homogenous melt). The results showed that the MAed AlCoFeMoNiTi HEA produced the VHS of 8.87 GPa whereas the AM sample exhibited 7.68 GPa VHS. This was due to retained fine grains and the formation of nano-precipitates (Fig. 36) in the sample processed by MA. Further, to understand the best consolidation techniques among SSP route, the comparison between VHP and SPS was done here from Liu et al.

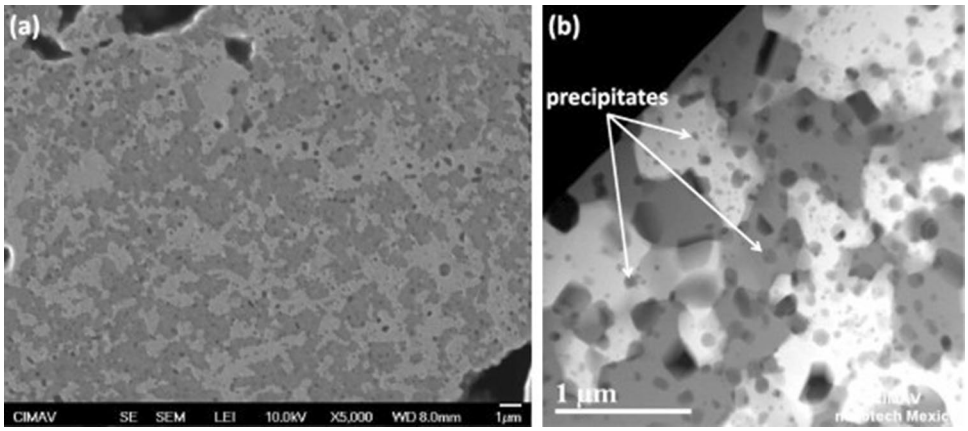

Fig. 36 Microstructure of sintered sample: **a** SEM, **b** TEM [49]

[109] and Ji et al. [110] works as an example. Liu et al. [109] have synthesized the cantor alloy (FeCoCrNiMn) powders using MA with BPR 15:1, speed of 255 rpm for 45 h under Ar atmosphere; then VHP sintering was carried out at different temperatures (850, 900, 950 and 1000 °C) with a constant pressure of 50 MPa for 1 h. The XRD pattern of HEA powders after MA has shown a major FCC phase and a small amount of BCC while the XRD pattern of HEA bulk sample after VHP sintering has shown only the FCC phase and a smaller amount of precipitates ($M_{23}C_6$ and M_7C_3) due to the control agent (N-heptane). This cantor alloy produced the YS of 1.652 GPa and VHS of 4.61 GPa sintered at 1173 K. On the other hand, Ji et al. [110] synthesized the same cantor alloy (FeCoCrNiMn) by MA (BPR 15:1, 255 rpm, 60 h) followed by SPS at 1073 K (50 MPa pressure, 10 min) under Ar gas. The bulk sample produced two different FCC phases [110] which yielded 1.987 GPa YS (highest value reported for FeCoCrNiMn HEA). Finally, the HEA powders can be directly coated on the products using TFD methods. Similarly, 3d printing technology can also be used to fabricate the HEA products directly.

HEAs are a new class of alloys which can be used in high-temperature applications with improved properties at high temperature by which highly costliest and high density super alloys materials can be replaced by HEAs. Some of the HEAs can be used in aircraft propulsion systems, gas turbine blades, and accessories, heat exchanger parts in nuclear industries, products for processing industries (cement, chemical and textile machinery parts). For instance, nickel-based superalloys possess superior corrosion resistance up to 400 °C. However, for these applications, HEAs, especially from refractory based HEAs, exhibits outstanding resistance against corrosion even up to 700 °C which indicates the performance from HEAs becomes doubled. Tungsten carbide (WC), titanium nitride, silicon abrasives, boron carbide are the major conventional materials that are being used for fabricating the machine tools and cutting tools. It can be replaced and proposed by HEAs, but, still, more research has to be carried out to check the feasibility of these kinds of applications. Further, gas turbine blades, vanes, disks require superior physical and mechanical properties. Especially, these products need high tensile strength and high resistance against failure at both room and elevated temperatures. These parts are highly critical one which needs to operate around 900 °C. For these applications, currently single-crystalline superalloys are being used which has a tensile strength of around 500 MPa at ~ 1000 °C and ductility around 10% at room temperature. However, the manufacturing cost towards the development of single-crystalline superalloys is highly expensive which is very difficult for controlling during its fabrications. Further, these parts require more creep resistance, fatigue strength, more thermal conductivity and good in environmental resistance. Hence, materials for these products should have lesser in the coefficient of thermal expansion and high value of elastic stiffness to eliminate deflections. In addition, currently, most of the turbine blades possess a specific strength of 570 Pa m^3/kg which should be operated for thousands of hours. Hence, the materials should have stabilized SS microstructures at high temperatures for which HEAs can be recommended, but, it has to be validated by conducting more research outcomes.

After deciding to choose HEAs for applications, next, the processing is the highly challenges. For example, when we prepare the HEAs through the melting route (LSP), it needs to have furnaces/equipment for operating at high temperatures. Further, these LSP route produces inhomogeneity in the form of segregation. Most of the parts produced from the melting route usually applied in as-cast conditions and or used after heat treatment with/without secondary operations (forming and metal cutting). As discussed in the previous sections, HEAs prepared by the LSP route produce more porosity and sometimes unwanted phases in the form of precipitates. Mostly, in the melting route, HEAs exhibits BCC, FCC, HCP, and some precipitates which mainly depend on the type of elements that are to be mixed, their atomic ratio, and other processing parameters. However, these unwanted

phases and incoherent precipices can be eliminated through SSP routes (PM) such as MA followed by SPS/HIP. Here, the necessary microstructural phases can be easily designed and controlled.

7 Conclusions

In this review article, several conventional and unconventional processing methods for the manufacturing of HEAs have been discussed elaborately and reported. Three extensive processing methods, namely, SSP, LSP, and TFD are explained with simple schematic by which the readers can and be able to understand the recent research works related to HEAs. Further, the influence and proper selection of processing parameters were reported in each processing method. The selection of processing methods is very much important as the performance of HEAs products mainly depends on processing methods and its parameters. The major features and issues related to the fabrication of HEAs were also investigated with appropriate sketches/microstructures. As far as SSP methods, MA followed by SPS can give improved properties whereas VAM, VIM, AM with EMS are the most common methods for manufacturing HEAs in liquid processing route due to its simplicity and its easiness. Further, the manufacturing of HEAs through advanced AMT was also discussed. In AMT, DLF and SLM are the best manufacturing techniques for fabricating HEAs. Moreover, various phase formation in each processing method, corresponding microstructural changes, and mechanical properties evolutions was also discussed with appropriate graphs/microstructures. Finally, the major challenges related to processing methods and applications of HEAs are also discussed and reported.

Acknowledgements The authors acknowledge the financial support of Qassim University under Deanship Research Grant of Saudi Arabia and provided research facilities to carry out this research work.

References

1. D.B. Miracle, J.D. Miller, O.N. Senkov, C. Woodward, M.D. Uchic, J. Tiley, Exploration and development of high entropy alloys for structural applications. Entropy **16**(1), 494–525 (2014)
2. Y. J. Huang, K.H. Chen, Master's Thesis, *Natl. Tsing Hua Univ.* (1996)
3. J. Yeh et al., Nanostructured high-entropy alloys with multiple principal elements: novel alloy design concepts and outcomes. Adv. Eng. Mater. **6**(5), 299–303 (2004)
4. C.-Y. Hsu, J.-W. Yeh, S.-K. Chen, T.-T. Shun, Wear resistance and high-temperature compression strength of Fcc CuCoNiCrAl 0.5 Fe alloy with boron addition. Metall. Mater. Trans. A **35**(5), 1465–1469 (2004)
5. Y. Jien-Wei, Recent progress in high entropy alloys. Ann. Chim. Sci. Mat **31**(6), 633–648 (2006)
6. J. Chen et al., A review on fundamental of high entropy alloys with promising high–temperature properties. J. Alloys Compd. **760**, 15–30 (2018)
7. T. Bhattacharjee et al., Effect of low temperature on tensile properties of AlCoCrFeNi2.1 eutectic high entropy alloy. Mater. Chem. Phys. **210**, 207–212 (2018)
8. Y.F. Ye, Q. Wang, J. Lu, C.T. Liu, Y. Yang, High-entropy alloy: challenges and prospects. Mater. Today **19**(6), 349–362 (2016)
9. P.F. Yu et al., The high-entropy alloys with high hardness and soft magnetic property prepared by mechanical alloying and high-pressure sintering. Intermetallics **70**, 82–87 (2016)
10. Y.Y.Y. Chen, T. Duval, U.D.D. Hung, J.W.W. Yeh, H.C.C. Shih, Microstructure and electrochemical properties of high entropy alloys—a comparison with type-304 stainless steel. Corros. Sci. **47**(9), 2257–2279 (2005)
11. L.J.J. Zhang et al., The microstructural evolution and hardness of the equiatomic CoCrCuFeNi high-entropy alloy in the semi-solid state. J. Alloys Compd. **745**, 75–83 (2018)
12. W. Huo et al., Ultrahigh hardness and high electrical resistivity in nano-twinned, nanocrystalline high-entropy alloy films. Appl. Surf. Sci. **439**, 222–225 (2018)
13. G. Jin et al., High temperature wear performance of laser-cladded FeNiCoAlCu high-entropy alloy coating. Appl. Surf. Sci. **445**, 113–122 (2018)
14. C. Shang, E. Axinte, W. Ge, Z. Zhang, Y. Wang, High-entropy alloy coatings with excellent mechanical, corrosion resistance and magnetic properties prepared by mechanical alloying and hot pressing sintering. Surfaces Interfaces **9**, 36–43 (2017)
15. K.V. Yusenko et al., High-pressure high-temperature tailoring of High Entropy Alloys for extreme environments. J. Alloys Compd. **738**, 491–500 (2018)
16. M.D.D. Cropper, Thin films of AlCrFeCoNiCu high-entropy alloy by pulsed laser deposition. Appl. Surf. Sci. **455**(May), 153–159 (2018)
17. S. Mohanty et al., Powder metallurgical processing of equiatomic AlCoCrFeNi high entropy alloy: microstructure and mechanical properties. Mater. Sci. Eng. A **679**, 299–313 (2017)
18. X.W. Qiu, Y.P. Zhang, L. He, C.G. Liu, Microstructure and corrosion resistance of AlCrFeCuCo high entropy alloy. J. Alloys Compd. **549**, 195–199 (2013)
19. R. Wang, W. Chen, J. Zhong, L. Zhang, Experimental and numerical studies on the sluggish diffusion in face centered cubic Co–Cr–Cu–Fe–Ni high-entropy alloys. J. Mater. Sci. Technol. **34**(10), 1791–1798 (2018)
20. K. Tsai, M. Tsai, J. Yeh, Sluggish diffusion in Co–Cr–Fe–Mn–Ni high-entropy alloys. Acta Mater. **61**(13), 4887–4897 (2013)
21. B.S. Murty, J.-W. Yeh, S. Ranganathan, P.P. Bhattacharjee, *High-Entropy Alloys* (Elsevier, Amsterdam, 2019)
22. K. Alagarsamy et al., Mechanical Properties of High Entropy Alloy Al 0.1 CoCrFeNi for Peripheral Vascular Stent Application. Cardiovasc. Eng. Technol. **7**(4), 448–454 (2016)
23. J. Li, W. Jia, J. Wang, H. Kou, D. Zhang, E. Beaugnon, Enhanced mechanical properties of a CoCrFeNi high entropy alloy by supercooling method. JMADE **95**, 183–187 (2016)
24. H.W. Yao, J.W. Qiao, J.A. Hawk, H.F. Zhou, M.W. Chen, M.C. Gao, Mechanical properties of refractory high-entropy alloys: experiments and modeling. J. Alloys Compd. **696**, 1139–1150 (2017)
25. C.C. Juan et al., Enhanced mechanical properties of HfMoTaTiZr and HfMoNbTaTiZr refractory high-entropy alloys. Intermetallics **62**, 76–83 (2015)
26. Y. Zhang et al., Microstructures and properties of high-entropy alloys. Prog. Mater. Sci. **61**, 1–93 (2013)

27. C. Li, Y. Zhou, Y. Xie, D. Zhou, D. Zhang, Effects of milling time and sintering temperature on structural evolution, densification behavior and properties of a W-20 wt% Cu alloy. J. Alloys Compd. **731**, 537–545 (2018)
28. M.D.D. Alcalá, C. Real, I. Fombella, I. Trigo, J.M.M. Córdoba, Effects of milling time, sintering temperature, Al content on the chemical nature, microhardness and microstructure of mechanochemically synthesized FeCoNiCrMn high entropy alloy. J. Alloys Compd. **749**, 834–843 (2018)
29. S.-H. Joo et al., Structure and properties of ultrafine-grained CoCrFeMnNi high-entropy alloys produced by mechanical alloying and spark plasma sintering. J. Alloys Compd. **698**, 591–604 (2017)
30. G.D.S.M.Z.J.R.G.C.L.C.-W.T.J.-W.Y.P.P. Bhattacharjee, Microstructure and texture evolution during annealing of equiatomic\nCoCrFeMnNi high-entropy alloy. J. Alloys Compd. **587**, 544–552 (2014)
31. T.T. Shun, Y.C. Du, Age hardening of the Al0.3CoCrFeNiC0.1high entropy alloy. J. Alloys Compd. **478**(1–2), 269–272 (2009)
32. A. Lawley, Atomization of specialty alloy powders. JOM **33**(1), 13–18 (1989)
33. R. Li, Y. Shi, Z. Wang, L. Wang, J. Liu, W. Jiang, Densification behavior of gas and water atomized 316L stainless steel powder during selective laser melting. Appl. Surf. Sci. **256**(13), 4350–4356 (2010)
34. C.C. Yang, J.L. Hang Chau, C.J. Weng, C.S. Chen, Y.H. Chou, Preparation of high-entropy AlCoCrCuFeNiSi alloy powders by gas atomization process. Mater. Chem. Phys. **202**, 151–158 (2017)
35. S. Zhou et al., Microstructure evolution of Al0. 6CoCrFeNi high entropy alloy powder prepared by high pressure gas atomization. Trans. Nonferrous Met. Soc. China **28**(5), 939–945 (2018)
36. D. Yim et al., Compaction behavior of water-atomized CoCrFeMnNi high-entropy alloy powders. Mater. Chem. Phys. **210**, 95–102 (2018)
37. Y. Liu, J. Wang, Q. Fang, B. Liu, Y. Wu, S. Chen, Preparation of superfine-grained high entropy alloy by spark plasma sintering gas atomized powder. Intermetallics **68**, 16–22 (2016)
38. J. Wang et al., Flow behavior and microstructures of powder metallurgical CrFeCoNiMo0. 2 high entropy alloy during high temperature deformation. Mater. Sci. Eng., A **689**, 233–242 (2017)
39. R. Clinktan, V. Senthil, K.R. Ramkumar, S. Sivasankaran, F.A. Al-Mufadi, Effect of boron carbide nano particles in CuSi4Zn14 silicone bronze nanocomposites on matrix powder surface morphology and structural evolution via mechanical alloying. Ceram. Int. **45**, 33492 (2018)
40. B. Madavali, J.-H. Lee, J.K. Lee, K.Y. Cho, S. Challapalli, S.-J. Hong, Effects of atmosphere and milling time on the coarsening of copper powders during mechanical milling. Powder Technol. **256**, 251–256 (2014)
41. F.T. Mahi, O.-H. Kwon, *Liquid Phase Sintering: Ceramics* (Elsevier, Amsterdam, 2016)
42. H. Cheng, X. Liu, Q. Tang, W. Wang, X. Yan, P. Dai, Microstructure and mechanical properties of FeCoCrNiMnAlx high-entropy alloys prepared by mechanical alloying and hot-pressed sintering. J. Alloys Compd. **775**, 742–751 (2019)
43. D. Oleszak, A. Antolak-dudka, T. Kulik, High entropy multicomponent WMoNbZrV alloy processed by mechanical alloying. Mater. Lett. **232**, 160–162 (2018)
44. A.I. Yurkova, V.V. Cherniavsky, V. Bolbut, M. Krüger, I. Bogomol, Structure formation and mechanical properties of the high-entropy AlCuNiFeCr alloy prepared by mechanical alloying and spark plasma sintering. J. Alloys Compd. **786**, 139–148 (2019)
45. A. Emamifar, B. Sadeghi, P. Cavaliere, H. Ziaei, Microstructural evolution and mechanical properties of AlCrFeNiCoC high entropy alloy produced via spark plasma sintering. Powder Metall. **62**(1), 61–70 (2019)
46. C. Suryanarayana, Mechanical alloying and milling. Prog. Mater Sci. **46**(1–2), 1–184 (2001)
47. F. Yuhu, Z. Yunpeng, G. Hongyan, S. Huimin, H. Li, Alnicrfexmo0. 2CoCu high entropy alloys prepared by powder metallurgy. Rare Met. Mater. Eng. **42**(6), 1127–1129 (2013)
48. V. Shivam, J. Basu, V.K. Pandey, Y. Shadangi, N.K. Mukhopadhyay, Alloying behaviour, thermal stability and phase evolution in quinary AlCoCrFeNi high entropy alloy. Adv. Powder Technol. **29**(9), 2221–2230 (2018)
49. F.J. Baldenebro-Lopez, J.M. Herrera-Ramírez, S.P. Arredondo-Rea, C.D. Gómez-Esparza, R. Martínez-Sánchez, Simultaneous effect of mechanical alloying and arc-melting processes in the microstructure and hardness of an AlCoFeMoNiTi high-entropy alloy. J. Alloys Compd. **643**, S250–S255 (2015)
50. C. Sun, P. Li, S. Xi, Y. Zhou, S. Li, X. Yang, A new type of high entropy alloy composite Fe18Ni23Co25Cr21Mo8WNb3C2 prepared by mechanical alloying and hot pressing sintering. Mater. Sci. Eng. A **728**, 144–150 (2018)
51. Z. Xu, M.A. Hodgson, P. Cao, A comparative study of powder metallurgical (PM) and wrought Fe–Mn–Si alloys. Mater. Sci. Eng., A **630**, 116–124 (2015)
52. Z. Fu et al., Microstructure and strengthening mechanisms in an FCC structured single-phase nanocrystalline Co25Ni25Fe25Al7. 5Cu17. 5 high-entropy alloy. Acta Mater. **107**, 59–71 (2016)
53. Z. Tang et al., Tensile ductility of an AlCoCrFeNi multi-phase high-entropy alloy through hot isostatic pressing (HIP) and homogenization. Mater. Sci. Eng., A **647**, 229–240 (2015)
54. L.F. Francis, Powder Processes, in *Materials Processing*, ed. by L.F.B.T.-M.P. Francis (Academic Press, Boston, 2016), pp. 343–414
55. Z. Fu, W. Chen, H. Wen, Z. Chen, E.J. Lavernia, Effects of Co and sintering method on microstructure and mechanical behavior of a high-entropy Al0. 6NiFeCrCo alloy prepared by powder metallurgy. J. Alloys Compd. **646**, 175–182 (2015)
56. N. Eißmann, B. Klöden, T. Weißgärber, B. Kieback, High-entropy alloy CoCrFeMnNi produced by powder metallurgy. Powder Metall. **60**(3), 184–197 (2017)
57. J. Pan, T. Dai, T. Lu, X. Ni, J. Dai, M. Li, Microstructure and mechanical properties of Nb25Mo25Ta25W25 and Ti8Nb23Mo23Ta23W23 high entropy alloys prepared by mechanical alloying and spark plasma sintering. Mater. Sci. Eng. A **738**, 362–366 (2018)
58. D. Yim, P. Sathiyamoorthi, S.-J. Hong, H.S. Kim, Fabrication and mechanical properties of TiC reinforced CoCrFeMnNi high-entropy alloy composite by water atomization and spark plasma sintering. J. Alloys Compd. **781**, 389–396 (2019)
59. S. Mohanty, N.P. Gurao, P. Padaikathan, K. Biswas, Ageing behaviour of equiatomic consolidated Al20Co20Cu20Ni20Zn20 high entropy alloy. Mater. Charact. **129**, 127–134 (2017)
60. K.B. Zhang, Z.Y. Fu, J.Y. Zhang, W.M. Wang, S.W. Lee, K. Niihara, Characterization of nanocrystalline CoCrFeNiTiAl high-entropy solid solution processed by mechanical alloying. J. Alloys Compd. **495**(1), 33–38 (2010)
61. R.S. Ganji, P.S. Karthik, K.B.S. Rao, K.V. Rajulapati, Strengthening mechanisms in equiatomic ultrafine grained AlCoCrCuFeNi high-entropy alloy studied by micro-and nanoindentation methods. Acta Mater. **125**, 58–68 (2017)

62. S.-J.L. Kang, S.-J.L. Kang, Basis of liquid phase sintering, in *Sintering*, ed. by S.-J.L.B.T.-S. Kang (Butterworth-Heinemann, Oxford, 2005), pp. 199–203
63. M.A. Hemphill et al., Fatigue behavior of Al0. 5CoCrCuFeNi high entropy alloys. Acta Mater. **60**(16), 5723–5734 (2012)
64. S. Singh, N. Wanderka, B.S. Murty, U. Glatzel, J. Banhart, Decomposition in multi-component AlCoCrCuFeNi high-entropy alloy. Acta Mater. **59**(1), 182–190 (2011)
65. F. Otto, N.L. Hanold, E.P. George, Microstructural evolution after thermomechanical processing in an equiatomic, single-phase CoCrFeMnNi high-entropy alloy with special focus on twin boundaries. Intermetallics **54**, 39–48 (2014)
66. L.C. Tsao, C.S. Chen, C.P. Chu, Age hardening reaction of the Al0.3CrFe1.5MnNi0.5 high entropy alloy. Mater. Des. **36**, 854–858 (2012)
67. M. Zhan, C. Gu, Z. Jiang, L. Hu, H. Yang, Application of ductile fracture criteria in spin-forming and tube-bending processes. Comput. Mater. Sci. **47**(2), 353–365 (2009)
68. L. Hou, J. Hui, Y. Yao, J. Chen, J. Liu, Effects of Boron Content on microstructure and mechanical properties of AlFeCoNiBx High Entropy Alloy Prepared by vacuum arc melting. Vacuum **164**, 212–218 (2019)
69. Y. Du, Y. Lu, T. Wang, T. Li, G. Zhang, Effect of electromagnetic stirring on microstructure and properties of Al0.5CoCrCuFeNi alloy. Procedia Eng. **27**(2011), 1129–1134 (2012)
70. H. Luo, Z. Li, A.M. Mingers, D. Raabe, Corrosion behavior of an equiatomic CoCrFeMnNi high-entropy alloy compared with 304 stainless steel in sulfuric acid solution. Corros. Sci. **134**, 131–139 (2018)
71. E. Fazakas, J.Q. Wang, V. Zadorozhnyy, L.K. Varga, Microstructural evolution and corrosion behavior of Al 25 Ti 25 Ga 25 Be 25 equi-molar composition alloy. Mater. Corros. **119049**(7), 691–695 (2014)
72. Y. Liu et al., Microstructure and mechanical properties of refractory HfMo0. 5NbTiV0. 5Six high-entropy composites. J. Alloys Compd. **694**, 869–876 (2017)
73. H. Qiu, H. Zhu, J. Zhang, Z. Xie, Effect of Fe content upon the microstructures and mechanical properties of FexCoNiCu high entropy alloys. Mater. Sci. Eng. A **769**, 138514 (2020)
74. D.G. Kim et al., Effects of annealing temperature on microstructures and tensile properties of a single FCC phase CoCuMnNi high-entropy alloy. J. Alloys Compd. **812**, 152111 (2020)
75. Z. Yao, Comparison of structures and properties of arc-melted and induction-melted high entropy alloys, *Master's thesis, Tampere Univ. Technol.* (2016)
76. H. Zheng et al., Transition of solid-liquid interface and tensile properties of CoCrFeNi high-entropy alloys during directional solidification. J. Alloys Compd. **787**, 1023–1031 (2019)
77. H. Zheng et al., Microstructure evolution, Cu segregation and tensile properties of CoCrFeNiCu high entropy alloy during directional solidification. J. Mater. Sci. Technol. **38**, 19–27 (2019)
78. S.T. Mileiko, S.A. Firstov, N.A. Novokhatskaya, V.F. Gorban, N.P. Krapivka, Oxide-fibre/high-entropy-alloy-matrix composites. Compos. Part A Appl. Sci. Manuf. **76**, 131–134 (2015)
79. F. He et al., Designing eutectic high entropy alloys of CoCrFeNiNbx. J. Alloys Compd. **656**, 284–289 (2016)
80. Y. Yu, F. He, Z. Qiao, Z. Wang, W. Liu, J. Yang, Effects of temperature and microstructure on the triblogical properties of CoCrFeNiNbx eutectic high entropy alloys. J. Alloys Compd. **775**, 1376–1385 (2019)
81. N.A. Khan et al., High entropy alloy thin films of AlCoCrCu05FeNi with controlled microstructure. Appl. Surf. Sci. **495**, 143560 (2019)
82. M. M. Hassan, 16—Antimicrobial Coatings for Textiles, A. B. T.-H. of A. C. Tiwari, Ed. Elsevier, 2018, pp. 321–355
83. J.A. Juhasz, S.M. Best, 6—Surface modification of biomaterials by calcium phosphate deposition, in *Woodhead Publishing Series in Biomaterials*, ed. by B. Williams (Woodhead Publishing, Cambridge, 2011), pp. 143–169
84. H. Kim et al., Mechanical and electrical properties of NbMoTaW refractory high-entropy alloy thin films. Int. J. Refract. Met. Hard Mater. **80**, 286–291 (2018)
85. J. Pou, F. Lusquiños, R. Comesaña, M. Boutinguiza, 14—Production of biomaterial coatings by laser-assisted processes, in *Woodhead Publishing Series in Welding and Other Joining Technologies*, ed. by J. Lawrence, J. Pou, D.K.Y. Low, L.M.P. Toyserkani (Woodhead Publishing, Cambridge, 2010), pp. 394–425
86. A. Michelmore, Thin film growth on biomaterial surfaces, in *Thin Film Coatings for Biomaterials and Biomedical Applications*, ed. by B.A. Griesser (Woodhead Publishing, Cambridge, 2016), pp. 29–47
87. T.-W. Lu et al., Microstructures and mechanical properties of CoCrFeNiAl0.3 high-entropy alloy thin films by pulsed laser deposition. Appl. Surf. Sci. **494**(May), 72–79 (2019)
88. K.C. Cheng, J.H. Chen, S. Stadler, S.H. Chen, Properties of atomized AlCoCrFeNi high-entropy alloy powders and their phase-adjustable coatings prepared via plasma spray process. Appl. Surf. Sci. **478**, 478–486 (2019)
89. V. Ocelik, N. Janssen, S.N. Smith, J.T.M. De Hosson, Additive manufacturing of high-entropy alloys by laser processing. JOM **68**(7), 1810–1818 (2016)
90. X. Li, Additive manufacturing of advanced multi-component alloys: bulk metallic glasses and high entropy alloys. Adv. Eng. Mater. **20**(5), 1700874 (2018)
91. R. Li, P. Niu, T. Yuan, P. Cao, C. Chen, K. Zhou, Selective laser melting of an equiatomic CoCrFeMnNi high-entropy alloy: processability, non-equilibrium microstructure and mechanical property. J. Alloys Compd. **746**, 125–134 (2018)
92. J. Joseph, P. Hodgson, T. Jarvis, X. Wu, N. Stanford, D. Mark, Effect of hot isostatic pressing on the microstructure and mechanical properties of additive manufactured Al x CoCrFeNi high entropy alloys. Mater. Sci. Eng. A **733**(May), 59–70 (2018)
93. R. Wang, K. Zhang, C. Davies, X. Wu, Evolution of microstructure, mechanical and corrosion properties of AlCoCrFeNi high-entropy alloy prepared by direct laser fabrication. J. Alloys Compd. **694**, 971–981 (2017)
94. Z.Y. Rao et al., Affordable FeCrNiMnCu high entropy alloys with excellent comprehensive tensile properties. Intermetallics **77**, 23–33 (2016)
95. C. Ni, Y. Shi, J. Liu, G. Huang, Characterization of Al0.5FeCu0.7NiCoCr high-entropy alloy coating on aluminum alloy by laser cladding. Opt. Laser Technol. J. **105**, 257–263 (2018)
96. J.B. Fogagnolo, F. Velasco, M.H. Robert, J.M. Torralba, Effect of mechanical alloying on the morphology, microstructure and properties of aluminium matrix composite powders. Mater. Sci. Eng. A **342**(1–2), 131–143 (2003)
97. R. M. Vilar, "Laser cladding," in *ALT'02 International Conference on Advanced Laser Technologies*, 2003, vol. 5147, pp. 385–392
98. E. Toyserkani, A. Khajepour, S.F. Corbin, *Laser cladding* (CRC Press, Boca Raton, 2004)
99. S.-K. Wong, T.-T. Shun, C.-H. Chang, C.-F. Lee, Microstructures and properties of Al0. 3CoCrFeNiMnx high-entropy alloys. Mater. Chem. Phys. **210**, 146–151 (2018)
100. B.D. Ratner, A.S. Hoffman, F.J. Schoen, J.E. Lemons, *Biomaterials science: an introduction to materials in medicine* (Elsevier, Amsterdam, 2004)
101. X. An, Q. Liu, B. Zheng, Microstructure and properties of laser cladding high entropy alloy MoFeCrTiWAlxSiy coating. Infra. Laser Eng **43**, 1140–1144 (2014)

102. T. Huang, L. Jiang, C. Zhang, H. Jiang, Y. Lu, T. Li, Effect of carbon addition on the microstructure and mechanical properties of CoCrFeNi high entropy alloy. Sci. China Technol. Sci. **61**(1), 117–123 (2018)
103. R.B. Nair, H.S. Arora, S. Mukherjee, S. Singh, H. Singh, H.S. Grewal, Exceptionally high cavitation erosion and corrosion resistance of a high entropy alloy. Ultrason. Sonochem. **41**, 252–260 (2018)
104. Z.D. Han et al., Microstructures and mechanical properties of TixNbMoTaW refractory high-entropy alloys. Mater. Sci. Eng. A **712**, 380–385 (2018)
105. N.N. Guo et al., Microstructure and mechanical properties of in situ MC-carbide particulates-reinforced refractory high-entropy Mo0. 5NbHf0. 5ZrTi matrix alloy composite. Intermetallics **69**, 74–77 (2016)
106. Z.D. Han et al., Effect of Ti additions on mechanical properties of NbMoTaW and VNbMoTaW refractory high entropy alloys. Intermetallics **84**, 153–157 (2017)
107. O.N. Senkov, S.V. Senkova, C. Woodward, Effect of aluminum on the microstructure and properties of two refractory high-entropy alloys. Acta Mater. **68**, 214–228 (2014)
108. O.N. Senkov, C. Woodward, D.B. Miracle, Microstructure and properties of aluminum-containing refractory high-entropy alloys. JOM **66**(10), 2030–2042 (2014)
109. X. Liu et al., Microstructure and mechanical properties of FeCoCrNiMnTi0.1C0.1 high-entropy alloy produced by mechanical alloying and vacuum hot pressing sintering. Vacuum **165**(7), 297–304 (2019)
110. W. Ji et al., Alloying behavior and novel properties of CoCrFeNiMn high-entropy alloy fabricated by mechanical alloying and spark plasma sintering. Intermetallics **56**, 24–27 (2015)
111. O.N. Senkov, J.M. Scott, S.V. Senkova, D.B. Miracle, C.F. Woodward, Microstructure and room temperature properties of a high-entropy TaNbHfZrTi alloy. J. Alloys Compd. **509**(20), 6043–6048 (2011)
112. S. Jiang, Z. Lin, H. Xu, Y. Sun, Studies on the microstructure and properties of AlxCoCrFeNiTi1-xhigh entropy alloys. J. Alloys Compd. **741**, 826–833 (2018)
113. P. Cui et al., Microstructure and mechanical behaviors of CoFeNiMnTixAl1-x high entropy alloys. Mater. Sci. Eng. A **731**, 124–130 (2018)
114. M. Zhang, L. Zhang, J. Fan, G. Li, P.K. Liaw, R. Liu, Microstructure and enhanced mechanical behavior of the Al7Co24Cr21Fe24Ni24 high-entropy alloy system by tuning the Cr content Mengdi. Mater Sci Eng A **733**, 299–306 (2018)
115. W. Wang, Z. Zhang, J. Niu, H. Wu, S. Zhai, Y. Wang, E ff ect of Al addition on structural evolution and mechanical properties of the Al x HfNbTiZr high-entropy alloys. Mater. Sci. Eng. A **16**, 242–249 (2018)
116. N.N. Guo et al., Microstructure and mechanical properties of refractory MoNbHfZrTi high-entropy alloy. Mater. Des. **81**, 87–94 (2015)
117. C. Zhang, C. Zhu, S. Shin, K. Vecchio, Enhancement of <001> recrystallization texture in non-equiatomic Fe–Ni–Co–Al-based high entropy alloys by combination of annealing and Cr addition. J. Alloys Compd. **768**, 277–286 (2018)
118. N.Y. Yurchenko, N.D. Stepanov, A.O. Gridneva, M.V. Mishunin, G.A. Salishchev, S.V. Zherebtsov, Effect of Cr and Zr on phase stability of refractory Al–Cr–Nb–Ti–V–Zr high-entropy alloys. J. Alloys Compd. **757**, 403–414 (2018)
119. S. Z. Z. Niu, H. C. C. Kou, J. Wang, and J. S. S. Li, Improved tensile properties of Al0.5CoCrFeNi high-entropy alloy by tailoring microstructures, *Rare Met.* 1–6 (2017)
120. É. Fazakas, J.Q. Wang, V. Zadorozhnyy, D.V. Louzguine-Luzgin, L.K. Varga, Microstructural evolution and corrosion behavior of Al25Ti25Ga25Be25 equi-molar composition alloy. Mater. Corros. **65**(7), 691–695 (2014)
121. X. Liu et al., Microstructure and mechanical properties of FeCoCrNiMnTi0. 1C0. 1 high-entropy alloy produced by mechanical alloying and vacuum hot pressing sintering. Vacuum **165**, 297–304 (2019)
122. O. Maulik, D. Kumar, S. Kumar, D.M. Fabijanic, V. Kumar, Structural evolution of spark plasma sintered AlFeCuCrMgx (x = 0, 0.5, 1, 1.7) high entropy alloys. Intermetallics **77**, 46–56 (2016)
123. X. Qiu, Microstructure, hardness and corrosion resistance of Al 2 CoCrCuFeNiTi x high-entropy alloy coatings prepared by rapid solidi fi cation. J. Alloys Compd. **735**, 359–364 (2018)
124. Y. Brif, M. Thomas, I. Todd, The use of high-entropy alloys in additive manufacturing. Scr. Mater. **99**, 93–96 (2015)